



## RESEARCH ARTICLE

Basin  
ResearchIAS  
EAGE

WILEY

# Thermal evolution and sediment provenance of the Cooper–Eromanga Basin: Insights from detrital apatite

Angus L. Nixon<sup>1,2</sup>  | Nicholas Fernie<sup>3</sup> | Stijn Glorie<sup>1,4</sup> | Martin Hand<sup>1,4</sup> | Betina Bendell<sup>5</sup> 

<sup>1</sup>School of Physics, Chemistry and Earth Sciences, Department of Earth Science, The University of Adelaide, Adelaide, South Australia, Australia

<sup>2</sup>AuScope Geochemistry Network, The University of Adelaide, Adelaide, South Australia, Australia

<sup>3</sup>Santos, Adelaide, South Australia, Australia

<sup>4</sup>Mineral Exploration Cooperative Research Centre, The University of Adelaide, Adelaide, South Australia, Australia

<sup>5</sup>Geological Survey of South Australia, Adelaide, South Australia, Australia

## Correspondence

Angus L. Nixon, School of Physics, Chemistry and Earth Sciences, Department of Earth Science, The University of Adelaide, Adelaide, SA 5005, Australia.  
Email: [angus.nixon@adelaide.edu.au](mailto:angus.nixon@adelaide.edu.au)

## Funding information

Australian Research Council

## Abstract

The prolific hydrocarbon and geothermal potential of the Cooper–Eromanga Basin has long been recognised and studied, however, the thermal history which underpins these resources has largely remained elusive. This study presents new apatite fission track and U–Pb data for eight wells within the southwestern domain of the Cooper–Eromanga Basin, from which thermal history and detrital provenance reconstructions were conducted. Samples taken from sedimentary rocks of the upper Eromanga Basin (Winton, Mackunda and Cadna-owie Formations) yield dominant Early-Cretaceous and minor Late-Permian–Triassic apatite U–Pb ages that are (within uncertainty) equivalent to corresponding fission track age populations. Furthermore, the obtained Cretaceous apatite ages correlate well with the stratigraphic ages for each analysed formation, suggesting (1) little time lag between apatite exposure in the source region and sediment deposition, and (2) that no significant (>ca. 100°C) reheating affected these formations in this region following deposition. Cretaceous apatites were likely distally sourced from an eastern Australian volcanic arc, (e.g. the Whitsunday Igneous Association), and mixed with Permian–Triassic sediment sources from the New England and/or Mossman Orogens. Deeper samples (>2000 m) from within the southwestern Cooper Basin yielded partially reset fission track ages, indicative of heating to temperatures exceeding ca. 100–80°C after deposition. The associated thermal history models are broadly consistent with previous studies and suggest that maximum temperatures were reached at ca. 100–70 Ma as a result of hydrothermal circulation correlating with high rates of sedimentation. Subsequent Late-Cretaceous–Palaeogene cooling is interpreted to reflect post magmatic thermal subsidence and cessation of hydrothermal activity, as well as potential modified rock thermal conductivity as a response to fluid flow. Five of the seven modelled wells record a Neogene heating event, the geological significance of which remains tentative but may suggest possible reactivation of the Cooper Hot Spot and associated hydrothermal circulation.

This is an open access article under the terms of the [Creative Commons Attribution](https://creativecommons.org/licenses/by/4.0/) License, which permits use, distribution and reproduction in any medium, provided the original work is properly cited.

© 2024 The Authors. *Basin Research* published by International Association of Sedimentologists and European Association of Geoscientists and Engineers and John Wiley & Sons Ltd.

## KEYWORDS

Cooper–Eromanga Basin, detrital apatite, hydrothermal circulation, provenance, Thermal history, Whitsunday Igneous Association

## 1 | INTRODUCTION

The Cooper–Eromanga Basin in central Australia is a largely non-marine sedimentary basin, which has remained one of Australia's most significant economic petroleum provinces for many decades (e.g. Gravestock et al., 1998). Consequently, the basin has been the subject of extensive research with relation to structural history, lithology, evolution of stress fields and geothermal gradients. However, relatively little work has been done to constrain the low-temperature thermal history of the basin. Understanding the evolution of the thermal regime in the basin has the potential to provide temporal constraints on the burial and thermal maturation history in the basin, which has important implications for petroleum and geothermal exploration (Armstrong, 2005; Beardsmore, 2004; Deighton & Hill, 1998; Mavromatidis, 2007; Röth & Littke, 2022). Previous studies have predicted a complex thermal history within the basin, suggesting elevated temperatures during the Early to middle Cretaceous, reaching a thermal peak at ca. 100–90 Ma, followed by a period of cooling before temperatures again increased to reach present day conditions since ca. 5–2 Ma (Duddy et al., 2002). Progressive sedimentation above abnormally high heat-producing granites of the Big Lake Suite which intrude the underlying Warburton Basin (Figure 1), hydrothermal activity and high basal heat flows have been suggested as mechanisms for significant post-burial heating in the middle Cretaceous, with Late-Cretaceous cooling attributed to a transition away from these regimes (Duddy et al., 2002; Röth & Littke, 2022). Subsequent Neogene reheating mechanisms, however, have proven more enigmatic, but may potentially be explained by hydrothermal processes within the basin (Deighton & Hill, 1998; Hardman et al., 2019; Röth & Littke, 2022).

In addition, the sedimentary provenance for the Cooper–Eromanga Basin has not been studied extensively. Previous whole-rock Sm–Nd and zircon U–Pb (ZUPb) studies have suggested contemporaneous volcanism at the eastern Australian margin as the primary sediment source for the upper Eromanga Basin (Boult et al., 1997; Tucker et al., 2016; Whitford et al., 1994). A noticeable similarity between radiometric and depositional ages of sediment from the upper Eromanga Basin may be explained by prolonged volcanism in the Whitsunday Igneous Association between ca. 135 and

### Highlights

- Apatite from the upper Eromanga Basin sourced from the Whitsunday Igneous Association and Tasmanide orogens.
- Cooper Eromanga Basin saw complex Mesozoic–Cenozoic thermal history with maximum temperatures in Cretaceous.
- Thermal history strongly influenced by hydrothermal circulation, likely including recent Neogene reheating.

90 Ma, coincident with the duration of sedimentation (Tucker et al., 2016), with volcanogenic material present both from ash fallout and marine and later fluvial transport (e.g. MacDonald et al., 2013; Röth, 2022). Furthermore, the extreme robustness of zircon to recycling events makes it a problematic mineral for obtaining first-cycle local provenance information (e.g. Chew et al., 2020).

This study aims to enhance the understanding of the thermal history and sediment provenance of the basin, through the application of combined apatite U–Pb (AUPb) and apatite fission track (AFT) analysis and low-temperature thermal history modelling. The AUPb ages constrain the timing at which the apatite crystals cooled below temperatures of ca. 550–350°C (Chew & Spikings, 2015). Within unmetamorphosed sedimentary rocks, AUPb ages generally hold complementary provenance information to the more traditional ZUPb ages (e.g. Glorie et al., 2020). However, since apatites can grow in both mafic and felsic sources (unlike zircons), the AUPb system is additionally able to trace mafic provenances (e.g. Gillespie et al., 2018; Pochon et al., 2016). Furthermore, apatite is generally superior at capturing first-cycle provenance information as compared to zircon (e.g. Chew et al., 2020). AFT ages reflect the time of cooling through temperatures of ca. 120–60°C (Gleadow et al., 1986; Wagner & Van den haute, 1992), which can hold either provenance (non-reset) or thermal history (partial reset) information. The combination of these two thermochronometers on the same grains allows for a full reconstruction of the source-to-sink and low-temperature thermal history of wells within the Cooper–Eromanga Basin.

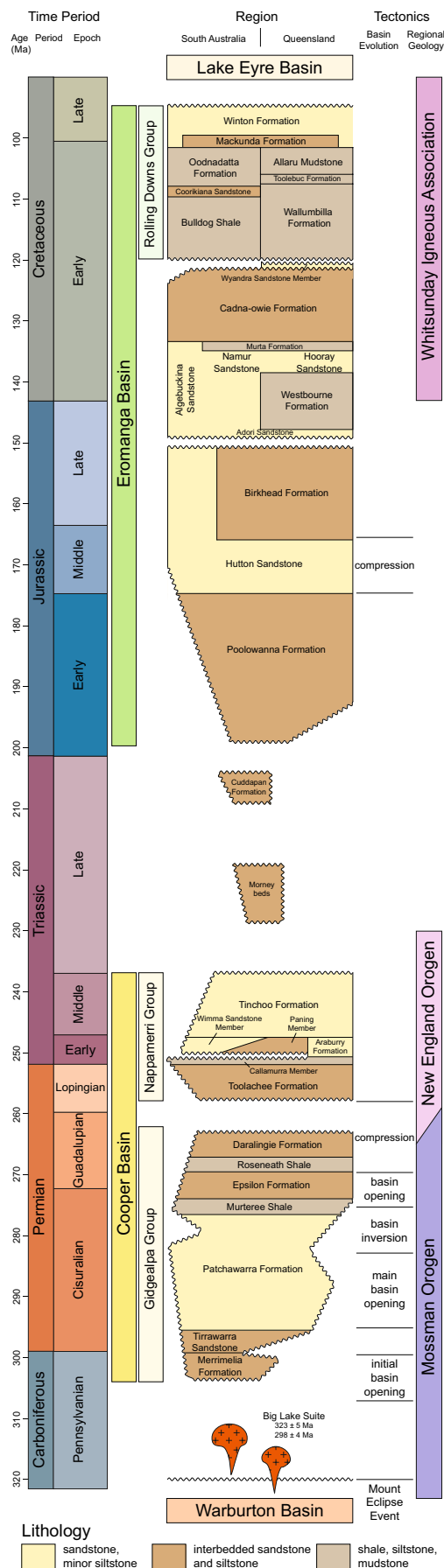


**FIGURE 1** Generalised stratigraphy of the Eromanga and Cooper Basins, modified after Hall et al. (2015, 2019), Bradshaw et al. (2022), Hannaford et al. (2022) and Röth and Littke (2022). Basin tectonic evolution after Röth and Littke (2022).

## 2 | GEOLOGICAL BACKGROUND

### 2.1 | Cooper Basin

The geographically overlapping Cooper and Eromanga basins are two constituents of a complex system of stacked sedimentary basins in central Australia. The basin system hosts major onshore petroleum reserves and is an intriguing geothermal prospect due to anomalously high geothermal gradients approaching up to 60°C/km (Hall et al., 2015). In South Australia, the Carboniferous–Triassic Cooper Basin is unconformable above the eastern extent of the Cambrian–Ordovician Warburton Basin (Figure 1). The Warburton Basin was intruded by highly radiogenic granites of the Big Lake Suite at ca. 330–295 Ma (Gatehouse et al., 1995), the age of which is constrained by limited geochronology. Cooper Basin sedimentary rocks were deposited in northeast-southwest trending troughs that developed during the Devonian–Carboniferous Alice Springs Orogeny (Alexander & Hibburt, 1996; Gravestock et al., 1998; Munson, 2014), initially in a glacial to periglacial environment before transitioning to fluvial and lacustrine environments (Alexander & Hibburt, 1996; Drexel & Preiss, 1995; Jadoon et al., 2017). The Cooper Basin reaches thicknesses in excess of 3000 m, however, due to the complex tectonic history (Röth & Littke, 2022) and variations of the palaeo-depositional environment (Gravestock et al., 1998) sedimentary thickness varies considerably and many units are not laterally continuous across the basin. The Cooper Basin is subdivided into two groups, the late-Permian–Triassic Nappamerri Group and the Late-Carboniferous–Permian Gidgealpa Group (Figure 1; Gravestock et al., 1998).

### 2.2 | Eromanga Basin

The intracratonic Jurassic–Cretaceous Eromanga Basin is laterally more extensive in size than the Cooper Basin, and completely covers the underlying Cooper Basin and much of central and eastern Australia (Figure 2a). Sedimentary rocks of the Eromanga Basin overlie the Cooper Basin above a major erosional unconformity, attributed to basin uplift in the waning stages of the Hunter-Bowen Orogeny (ca. 265–235 Ma; Gravestock et al., 1998; Hall et al., 2015; Li et al., 2012). Deposition in the Eromanga

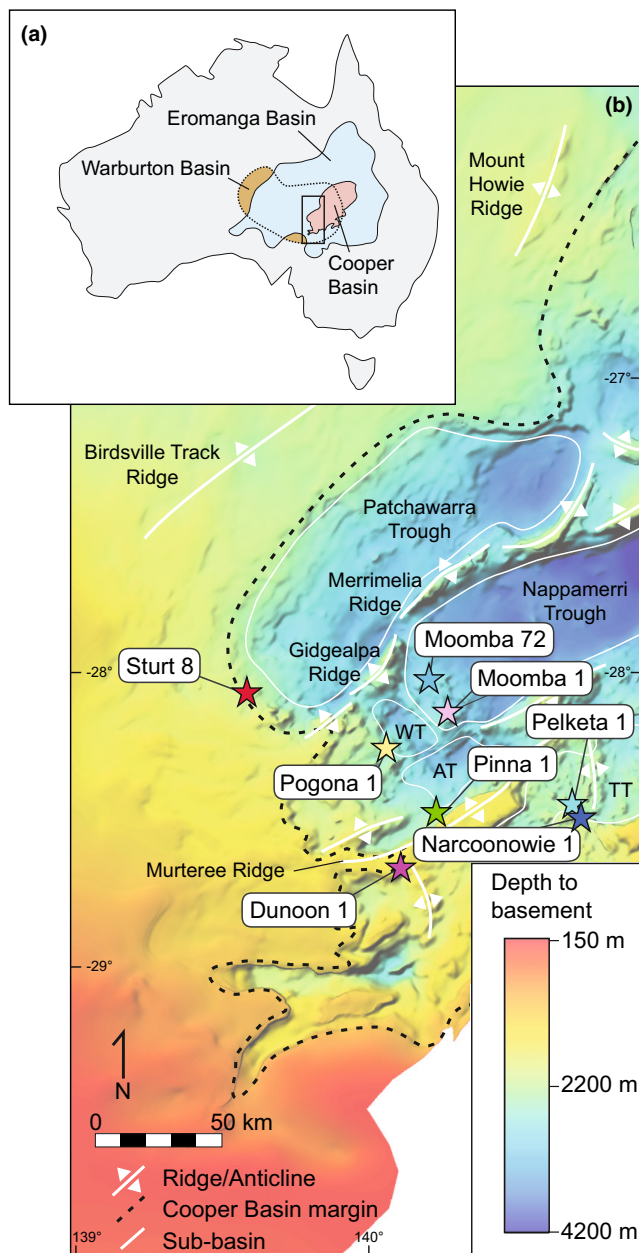


**FIGURE 2** (a) Locations of the stacked Warburton, Cooper and Eromanga Basins in Australia. Study area in (b) is shown by the black rectangle; (b) depth to pre-Permian basement below the Cooper–Eromanga Basin in South Australia. Locations of sampled wells and major structural features have been marked, as has the boundary of Cooper Basin, with abbreviations given as follows: AT, Allunga Trough; TT, Tenappera Trough; WT, Wooloo Trough. Depth to basement map sourced from Geological Survey of South Australia (2022), and major structural features adapted from Hall et al. (2015).

Basin began in the Early-Jurassic and continued until the Late-Cretaceous as the basin experienced progressive subsidence (Veevers, 2000), in a combination of fluvial, lacustrine and marine environments (Alexander & Hibburt, 1996). The transition from subsidence to uplift in central Australia in the Late-Cretaceous ca. 90 Ma

caused the termination of sedimentation and onset of erosion within the Eromanga Basin (Idnurm & Senoir, 1978; O'Sullivan et al., 1995).

The Eromanga Basin is subdivided into a number of lithostratigraphic units, spanning from the Early-Jurassic Poolawanna Formation to the Late-Cretaceous Winton Formation. Of units discussed in detail in this study, the Namur Sandstone was deposited in the Early-Cretaceous, and is described as a fluvial white to pale-grey, fine to coarse sandstone, containing minor siltstone and claystone interbeds (Alexander & Hibburt, 1996; Bradshaw et al., 2022; Hannaford et al., 2022). The Cadna-owie Formation was deposited in the Neocomian period of the Cretaceous and is described as a non-marine to marginal marine, coarsening-upward pale-grey siltstone, with minor fine-grained sandstone interbeds and occasional carbonaceous claystone (Alexander & Hibburt, 1996). The Oodnadatta Formation was deposited in the Albian and is described as a low-energy shallow marine deposit containing thinly bedded claystone, siltstone and fine sandstone (Alexander & Hibburt, 1996). The Cenomanian Mackunda Formation is a partially calcareous, very fine-grained sandstone siltstone and shale, which has been interpreted to have been deposited in alternating deep marine and shore face environments during several cycles of marine transgression and regression (Alexander & Hibburt, 1996). The temporally equivalent Winton Formation is a fine to coarse interbedded sandstone deposited in an east to west travelling fluvial system, which contains abundant volcanogenic debris, lithics, feldspars and traces of apatite (Alexander & Hibburt, 1996; Senior et al., 1978). These formations have both been interpreted by Veevers (1984) as sourced from the final pulse of volcanic activity by the eastern Australian magmatic arc. Sedimentary rocks of the Eromanga Basin are unconformably overlain by the Eocene–Quaternary non-marine Lake Eyre Basin (Figure 1; Alexander & Hibburt, 1996; Mavromatidis, 2006, 2007).

## 2.3 | Structural evolution

Numerous shifts in the regional stress regime since initial deposition during Adelaidean extension (ca. 650–540 Ma) have caused significant structural complexities within the Cooper–Eromanga Basin (Haines et al., 2001; Kulikowski et al., 2016). Late-Neoproterozoic extension induced the propagation of regional northeast-southwest striking normal faults within the underlying Warburton Basin and basement. Subsequent reactivation of these faults has strongly contributed to the development of the present-day basin geometries, forming the Gidgealpa and Murteree



Ridges that separate the three major troughs within the basin; the Patchwarra Trough, Nappamerri Trough and Tenappera Trough (Figure 2b; Apak et al., 1997; Kulikowski & Amrouch, 2017, 2018). Six major structural events have been proposed for the Cooper–Eromanga Basin, and comprise of (1) initial basin opening in the Pennsylvanian, (2) main phase of Cooper Basin formation during the early Permian, (3) subsequent basin inversion and ridge formation in the early Permian, (4) continuation of pull-apart basin formation in the middle Permian, (5) compression in the late Permian, and (6) initiation of SSE directed shearing in the Middle-Jurassic (Figure 1; Apak et al., 1997; Kulikowski & Amrouch, 2017, 2018; Reynolds et al., 2006; Röth & Littke, 2022). Compression and uplift in central Australia during the Late-Cretaceous led to erosion of the upper Eromanga sequence and substantial sediment thickening and folding within the Nappamerri Trough, particularly towards the northeast of the basin (Kulikowski & Amrouch, 2018; Mavromatidis, 2008; Mavromatidis & Hillis, 2005).

## 2.4 | Thermal history

The Cooper–Eromanga Basin has experienced a complex thermal history which is yet to be fully resolved, and still retains a globally unusual thermal structure. Previous thermal history reconstructions for the Cooper–Eromanga Basin conducted by Duddy and Moore (1999) and Duddy et al. (2002) using a combination of AFT, zircon fission track (ZFT) and vitrinite reflectance (VR) data have proposed that the temperature in the basin increased slowly with burial from the Permian to middle-Cretaceous, before increasing sharply to reach maximum palaeotemperatures at ca. 97–75 Ma. More recent studies have proposed an abrupt thermal maximum was reached ca. 100 Ma, which rapidly decayed and returned to stable conditions by ca. 70 Ma, with heating attributed to hydrothermal circulation and rapid sedimentation reaching rates of 200 m/Ma (Röth, 2022; Röth & Littke, 2022).

At present day, the Cooper–Eromanga Basin hosts anomalously high geothermal gradients, particularly in the Cooper Basin region and often above granitic basement (Beardsmore, 2004; Meixner et al., 2014; Siégl et al., 2012, 2018; Siégl et al., 2014). The Great Artesian Basin, hosted within aquifers of in the Eromanga Basin, additionally hosts high-temperature groundwaters which are globally anomalous (Polak & Horsfall, 1979). The cause of such elevated temperatures is yet to be fully resolved, but has in part been attributed to bottom-up factors such as the presence of highly radiogenic basement such as the Big Lake Suite granites (Beardsmore, 2004; Middleton, 1979) and silicic deep crust enriched in heat-producing elements

(Siégl et al., 2012, 2018), particularly in the region of the Thomson Orogen. Thermochronological studies, however, have suggested these elevated temperatures may be a relatively recent phenomenon. Neogene heating (ca. 5–2 Ma) across the basin has been recognised from detrital AFT data (Duddy et al., 2002; Duddy & Moore, 1999) and  $^{40}\text{Ar}/^{39}\text{Ar}$  data from Big Lake Suite granites (McLaren et al., 2006), although no robust explanation has yet been identified. Recurrent hydrothermal activity within the basin, augmented by local magmatism, however, may suggest another recent change to hydrothermal or ground-water systems as responsible for the observed Neogene thermal perturbations (Deighton & Hill, 1998; Röth & Littke, 2022).

## 2.5 | Sedimentary provenance

Provenance of the Cooper–Eromanga Basin sedimentary rocks has, to date, been poorly studied, with only a relatively small number of detrital radiometric ages published. Analysis of detrital zircons from the Winton Formation in the Eromanga Basin (stratigraphic age ca. 101–94 Ma; Bradshaw et al., 2022; Hannaford et al., 2022) from northeastern Queensland by Tucker et al. (2016) yielded prominent ZUPb age peaks between ca. 134 and 94 Ma, as well as minor age peaks ranging from the Triassic to Mesoproterozoic. Youngest Cretaceous zircon ages overlap with the depositional age of the formation, and coincide with major pulses of volcanism in the Whitsunday Igneous Association (Ewart et al., 1992). Minor sediment input was additionally sourced from igneous rocks associated with the New England Orogeny, Thomson Orogeny, Musgrave Province or detritus recycled by Tasmanide orogens (Tucker et al., 2016). Detrital ZUPb ages from the Mackunda Formation (stratigraphic age ca. 102–94 Ma; Bradshaw et al., 2022; Hannaford et al., 2022) have shown no evidence of syn-depositional provenance, with the youngest observed age peak occurring at ca. 133 Ma (Tucker et al., 2016). The Mackunda Formation does, however, show evidence of older populations, similar to those observed in the Winton Formation.

Detrital zircons from the Namur Sandstone (stratigraphic age ca. 144–130 Ma; Bradshaw et al., 2022; Hannaford et al., 2022) have yielded age populations significantly older than those of the Winton and Mackunda Formations, with major age peaks in the Cambrian and Mesoproterozoic (Stephens et al., 2017). Sediment provenance has been attributed to the Tasmanide orogens, with additional contributions from proximal basement outcrops. The stratigraphically underlying Birkhead Formation (stratigraphic age ca. 165–149 Ma; Bradshaw et al., 2022; Hannaford et al., 2022) is dominated by approximately

syn-sedimentary volcanogenic zircons from an east Australian arc (Boult et al., 1997). The underlying Hutton Sandstone (stratigraphic age ca. 175–165 Ma; Bradshaw et al., 2022; Hannaford et al., 2022) appears to lack volcanogenic input, with clasts attributed to a cratonic provenance (Boult et al., 1997; Watts, 1987). Collectively, this suggests the emergence of a volcanic arc system off eastern Australia in the Late-Jurassic which began to deliver volcanogenic sediment to the Birkhead Formation through a meandering fluvial system, superseding the braided fluvial system proposed to transport primarily continental detritus to the Hutton Sandstone (Boult et al., 1997).

No radiometric data currently exist for the Merrimelia Formation (stratigraphic age ca. 304–297 Ma; Hall et al., 2015, 2019), which was deposited in a complex glacial to glacio-lacustrine environment with additional aeolian sequences, and may therefore reflect a wide array of detrital provenance regions. Available interpretations of sedimentary clasts by Chaney et al. (1997), however, suggest that the majority of sediment in this formation was sourced

from intra-basinal material, derived from the underlying Warburton Basin. Minor distal sediment was likely derived from detritus shed during uplift associated with the central Australian Alice Springs or Petermann orogenies.

## 2.6 | Sample locations

Samples were taken from cuttings and core from eight wells located on structural highs in the Cooper–Eromanga Basin (Figure 2b; Table 1). Two sampled wells, Moomba 1 and Moomba 72, are located on the western margin of the Nappamerri Trough, in an area dominated by subsurface Carboniferous granites from the Big Lake Suite. These granites represent the local basement lithology in this trough and are often intersected by wells (Beardsmore, 2004; Gatehouse et al., 1995). The Pogona 1 and Sturt 8 wells are situated on the south-western margin of the Wooloo Trough and Patchawarra Trough respectively. In these wells, basal Cooper Basin sedimentary rocks also directly overlie basement granites from

**TABLE 1** Sample locations and stratigraphic units sampled, sorted by depth (provided as measured downhole depth). All coordinates are provided in the GDA94 system. Depth is provided as measured downhole depth. All samples were obtained from cuttings with the exception of sample M1-5 which was sampled from core.

Sample	Well	Latitude	Longitude	Unit	Depth top (m)	Depth bottom (m)
Du1-1	Dunoon 1	−28.6594	140.1088	Winton Formation	283.46	374.90
St8-1	Sturt 8	−28.1337	139.5835	Winton Formation	335.28	457.20
Pi1-1	Pinna 1	−28.4797	140.2549	Winton Formation	371.86	435.86
M72-1	Moomba 72	−28.0251	140.2053	Winton Formation	381.0	487.68
Na1-1	Narcoonowie 1	−28.4894	140.7242	Winton Formation	594.36	685.80
Du1-2	Dunoon 1	−28.6594	140.1088	Oodnadatta Formation	621.79	685.80
Po1-1	Pogona 1	−28.2614	140.0629	Winton Formation	685.80	795.53
Pi1-2	Pinna 1	−28.4797	140.2549	Mackunda Formation	746.76	810.77
M72-2	Moomba 72	−28.0251	140.2053	Winton Formation	914.40	1005.84
Po1-2	Pogona 1	−28.2614	140.0629	Mackunda Formation	923.54	1005.84
Du1-4	Dunoon 1	−28.6594	140.1088	Namur Sandstone	1207.01	1237.49
Na1-2	Narcoonowie 1	−28.4894	140.7242	Cadna-owie Formation	1283.51	1321.61
Pe1-1	Pelketa 1	−28.4434	140.6940	Cadna-owie Formation	1310.64	1341.12
St8-2	Sturt 8	−28.1337	139.5835	Cadna-owie Formation	1313.69	1350.26
Pi1-3	Pinna 1	−28.4797	140.2549	Cadna-owie Formation	1328.93	1359.41
Na1-3	Narcoonowie 1	−28.4894	140.7242	Namur Sandstone	1382.57	1437.44
Du1-6	Dunoon 1	−28.6594	140.1088	Hutton Sandstone	1417.32	1441.70
Pi1-4	Pinna 1	−28.4797	140.2549	Namur Sandstone	1450.85	1484.38
Na1-4	Narcoonowie 1	−28.4894	140.7242	Adori Sandstone	1497.48	1582.52
Po1-3	Pogona 1	−28.2614	140.0629	Cadna-owie Formation	1554.78	1610.87
M1-1	Moomba 1	−28.1513	140.2691	Cadna-owie Formation	1618.49	1685.24
Na1-6	Narcoonowie 1	−28.4894	140.7242	Narcoonowie Formation	1871.47	1886.71
Po1-6	Pogona 1	−28.2614	140.0629	Toolachee Formation	2148.84	2188.46
M1-5	Moomba 1	−28.1513	140.2691	Toolachee Formation	2317.94	2318.40

the Big Lake Suite (Gatehouse et al., 1995; Ostler, 1990; Turner, 1991). The Pinna 1 well is located on the southern margin of the Allunga Trough and terminates in a meta-siltstone unit within the Warburton Basin (Moore & Elliott, 1980). The Pelketa 1 and Narcoonowie 1 wells are situated southeast of the eastern edge of the Murteree Ridge. Pelketa 1 intersects and terminates within metasediments presumed to be of Ordovician age from the Warburton Basin (Schwebel, 1980). The Narcoonowie 1 well terminates in a late Cambrian orthoquartzite of the Warburton Basin (Frears, 1978). The Dunoon 1 well is the shallowest sampled well, located on the south of the western edge of the Murteree Ridge, and does not intersect Cooper Basin sediments (Beech, 1985). Present day thermal gradients of sampled wells were constrained between ca. 53 and 42°C/km as assessed during well completion (Beech, 1985; Frears, 1978; Moore & Elliott, 1980; Ostler, 1990, 1993; Schwebel, 1980; Turner, 1991).

### 3 | METHODS

#### 3.1 | Sample preparation and analysis

Apatite samples were prepared using conventional methods for fission track and U–Pb laser-ablation analysis (e.g. Glorie et al., 2017). Mineral separation was performed using a combination of magnetic and heavy liquid processing, and apatite grains mounted in EpoxyCure resin. Samples were etched in a solution of 5 M HNO<sub>3</sub> at 20 ± 0.5°C for 20 ± 0.5 s to reveal fission tracks. Apatite grains were imaged on a Zeiss AXIO Imager M2m Autoscan System and surface track densities were measured using FastTracks v3.0.19 software (Gleadow et al., 2009).

Analysis for U, Pb, Cl and rare-earth elements (REEs) was conducted using laser ablation inductively coupled plasma mass spectrometry (LA–ICP–MS) on a New Wave-213 laser connected to an Agilent 7900x mass spectrometer (analytical details provided in Appendix S1). Data collection was performed over three analytical sessions, with standard blocks interspaced within unknowns. Data reduction was performed with Iolite software (Paton et al., 2011) using Madagascar apatite as the primary standard for U–Pb analysis, and NIST610 as the primary standard for AFT and REE analysis. McClure and Durango apatite were used as secondary standards.

Following laser ablation, mounts were repolished to remove all etched tracks and laser damage, and irradiated with a <sup>252</sup>Cf source at the University of Melbourne to increase the likelihood of revealing confined tracks (Donelick & Miller, 1991) for use in thermal history modelling. The irradiated samples were subsequently etched, imaged and measured for their confined track lengths using identical protocols as for initial fission track analysis.

#### 3.2 | Apatite fission track thermochronology

AFT ages were calculated using the LA–ICP–MS method to obtain single-grain <sup>238</sup>U concentrations and fission track densities, using a session-specific zeta calibration from matched analysis of a Durango apatite standard (Vermeesch, 2017). All single-grain and population ages were calculated using the open source IsoplotR software (Vermeesch, 2018).

Thermal history modelling was performed using QTQt 5.5.0 software (Gallagher, 2012) with modelling inputs of single-grain AFT ages (and associated uncertainties), confined track lengths and single-grain Cl concentrations. Multiple samples from individual wells were modelled across depth profiles, constrained to present day depth, to produce internally consistent models. In addition to fission track data, existing VR data from samples at comparable depths to the analysed samples was used in the modelling protocols to constrain the maximum heating temperatures, where available (VR data sourced from Geological Survey of South Australia, 2022; provided in Appendix S1). Each individual sample was constrained to present-day temperatures as calculated from the current well geothermal gradient, and constrained at 18 ± 5°C at the stratigraphic age to represent surface temperatures at the time of deposition. All modelling parameters are outlined in Appendix S1, following guidelines outlined in Flowers et al. (2015).

#### 3.3 | Apatite U–Pb geochronology

AUPb ages were calculated using isochron regressions of isotopic ratios within Tera–Wasserburg concordia plots produced using IsoplotR software (Vermeesch, 2018). The lower intercept age is reported as the preferred AUPb age where samples exhibited sufficient spread in ratios for reliable regressions. As detrital samples may commonly preserve multiple age populations, age peaks have been identified using a combination of isotopic ratios and corresponding single-grain AFT ages (further discussion below and in Appendix S1).

### 4 | OBSERVATIONS AND RESULTS

#### 4.1 | Apatite U–Pb

##### 4.1.1 | Data accuracy

Secondary standards of Durango and McClure apatite were analysed interspaced with the unknown apatite samples to verify session accuracy for the U–Pb data.

Durango apatite returned  $^{207}\text{Pb}$  corrected  $^{238}\text{U}/^{206}\text{Pb}$  weighted mean ages of  $32.1 \pm 0.4$  Ma (session LA-2017),  $30.5 \pm 0.7$  Ma (session LA-2018a) and  $30.3 \pm 1.1$  Ma (session LA-2018b), while McClure apatite standards returned weighted mean ages of  $521 \pm 4$  Ma (session LA-2017),  $521 \pm 4$  Ma (session LA-2018a) and  $524 \pm 8$  Ma (session LA-2018b). These ages are in close agreement with a published Durango ( $^{40}\text{Ar}/^{39}\text{Ar}$  age  $31.44 \pm 0.18$  Ma; McDowell et al., 2005; AUPb age  $32.2 \pm 0.5$  Ma; Chew et al., 2014) and McClure apatite reference ages (AUPb age  $524.6 \pm 3.2$  Ma; Chew et al., 2014), respectively. Secondary standard age plots are provided in Appendix S1.

#### 4.1.2 | Eromanga Basin

Sixteen detrital apatite samples were analysed from multiple formations from the Eromanga Basin. Tera-Wasserburg

concordia plots for grains of these formations demonstrate spread which cannot be resolved by a single common-Pb regression (Figure 3), hence multiple detrital age populations appear to be present. In each formation with sufficient grain numbers for meaningful regression, the majority of grains define the youngest population within the unit, henceforth referred to as the 'primary' population. Where 'outliers' from the primary population define an auxiliary common-Pb regression (MSWD  $\approx 2$ –1) these populations are referred to as a separate 'secondary' population. Unfortunately, apatite geochemistry signatures do not differ significantly between grains of different AUPb populations, hence are of little use as an additional discrimination tool (Appendix S1).

##### 4.1.2.1 | Primary AUPb population

The majority of grains from each formation plot along a single regression line and define a (primary) AUPb age population (Figure 3; Table 2). For all formations

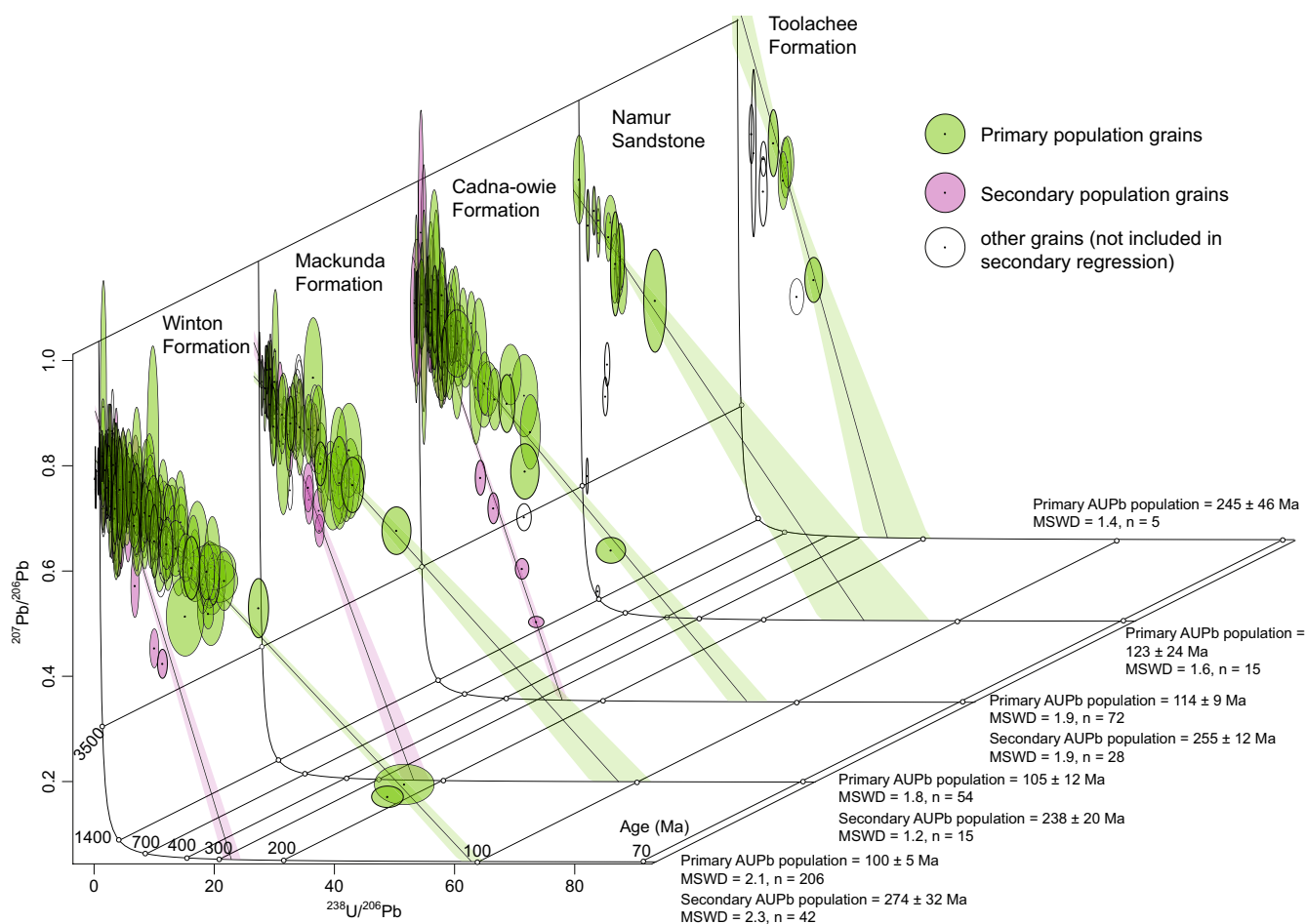


**FIGURE 3** Pooled Tera-Wasserburg concordia plots for detrital apatites from highly sampled stratigraphic units. Grains have been split by age population, as derived by a combination U–Pb ratio and single-grain AFT age. The 'primary' populations have been defined as the youngest population present within each unit, while 'secondary' populations have been derived via regression through older grains which satisfy a single isochron. Additional grains within each unit not clearly attributed to primary or secondary populations have been included and shown as unfilled ellipses. Linear regressions and age calculations for individual samples referenced in text are shown in Appendix S1.



**TABLE 2** Pooled formation apatite U–Pb population ages as calculated from linear regression in Tera–Wasserburg concordias. *N* denotes the number of grains used in age calculation, with all errors provided as two standard deviations. Stratigraphic ages based on framework of Hall et al. (2015, 2019), Bradshaw et al. (2022) and Hannaford et al. (2022). Individual Tera–Wasserburg concordia plots are provided in Appendix S1.

Unit	Stratigraphic age (Ma)	Primary AUPb age (Ma)	<i>N</i>	MSWD	Secondary AUPb age (Ma)	<i>N</i>	MSWD
Winton Formation	ca. 101–94	100 ± 5	206	2.1	274 ± 32	42	2.3
Mackunda Formation	ca. 102–94	105 ± 12	54	18	238 ± 20	15	1.2
Cadna-owie Formation	ca. 134–121	114 ± 9	72	1.9	255 ± 12	28	1.9
Namur Sandstone	ca. 144–130	123 ± 24	15	1.6	—	—	—
Toolachee Formation	ca. 258–252	245 ± 46	5	1.4	—	—	—

which allowed for reliable regression ( $\text{MSWD} \approx 2$ –1), the resulting primary AUPb ages were within uncertainty of the reported depositional age of the host sedimentary formation (Figures 4–6). The Winton Formation (stratigraphic age ca. 101–94 Ma; Bradshaw et al., 2022; Hannaford et al., 2022) yields a primary AUPb population at  $100 \pm 5$  Ma (Figure 3), while the Mackunda Formation (stratigraphic age ca. 102–94 Ma; Bradshaw et al., 2022; Hannaford et al., 2022) yielded a similar primary AUPb population of  $105 \pm 12$  Ma. The Cadna-owie Formation (stratigraphic age ca. 134–121 Ma; Bradshaw et al., 2022; Hannaford et al., 2022) yielded a primary AUPb population at  $114 \pm 9$  Ma, and the Namur Sandstone (stratigraphic age ca. 144–130 Ma; Bradshaw et al., 2022; Hannaford et al., 2022) yielded a primary AUPb age at  $123 \pm 24$  Ma (Figure 3). In some cases, samples with sufficient variation in U/Pb ratios allow for interpretation of AUPb age populations within individual samples, as provided in Appendix S1. However, these age populations are consistent with those derived for the encompassing formations while generally recording lower precision, hence grouped formation population ages have been quoted here for further discussion. Additional samples from the Oodnadatta Formation (stratigraphic age ca. 108–102 Ma; Bradshaw et al., 2022; Hannaford et al., 2022), Adori Sandstone (stratigraphic age ca. 150–148 Ma; Bradshaw et al., 2022; Hannaford et al., 2022) and Hutton Sandstone (stratigraphic age ca. 175–165 Ma; Bradshaw et al., 2022; Hannaford et al., 2022) yielded few detrital apatites, and AUPb ages were unable to be derived due to the low number of grains present and low U and radiogenic Pb within these apatites.

#### 4.1.2.2 | Secondary AUPb population

Some samples additionally contained detrital grains that define older (secondary) AUPb age populations (Figure 3; Table 2), although in some cases, these grains were too scattered or yielded insufficient radiogenic Pb for reliable age calculations. The Winton Formation (stratigraphic age ca.

101–94 Ma; Bradshaw et al., 2022; Hannaford et al., 2022) yielded a secondary AUPb population of  $274 \pm 32$  Ma. The Mackunda Formation (stratigraphic age ca. 102–94 Ma; Bradshaw et al., 2022; Hannaford et al., 2022) yielded a secondary AUPb population of  $238 \pm 20$  Ma, while the and Cadna-owie Formation (stratigraphic age ca. 134–121 Ma; Bradshaw et al., 2022; Hannaford et al., 2022) yielded a similar population of  $255 \pm 12$  Ma (Figure 3). These samples also contain additional grains which do not fall within either the primary or secondary AUPb populations, however, no reliable AUPb ages were able to be calculated for these grains and they are not discussed further. Similarly, grains diverging from the primary AUPb age population were also observed within samples from the Mackunda Formation, Oodnadatta Formation, Namur Sandstone, Adori Sandstone, Hutton Sandstone and Toolachee Formation, although no AUPb ages were able to be calculated for these populations.

#### 4.1.2.3 | Cooper Basin

Detrital apatite was sparse in Cooper Basin samples examined in this study, with only two samples from the basin able to be analysed for AUPb. Both samples were obtained from the Toolachee Formation (stratigraphic age ca. 258–252 Ma; Hall et al., 2015, 2019) which yielded a primary AUPb population at  $245 \pm 46$  Ma (Figure 3), which is within uncertainty of the stratigraphic age of this sample. Additional grains lie to the left of this Tera–Wasserburg regression (Figure 3), suggesting the presence of older detrital populations within the formation, although the ages of these grains are unable to be confidently resolved.

## 4.2 | Apatite fission track

### 4.2.1 | Data accuracy

Single-grain AFT ages were corrected with a zeta calibration derived using Durango apatite standards interspaced

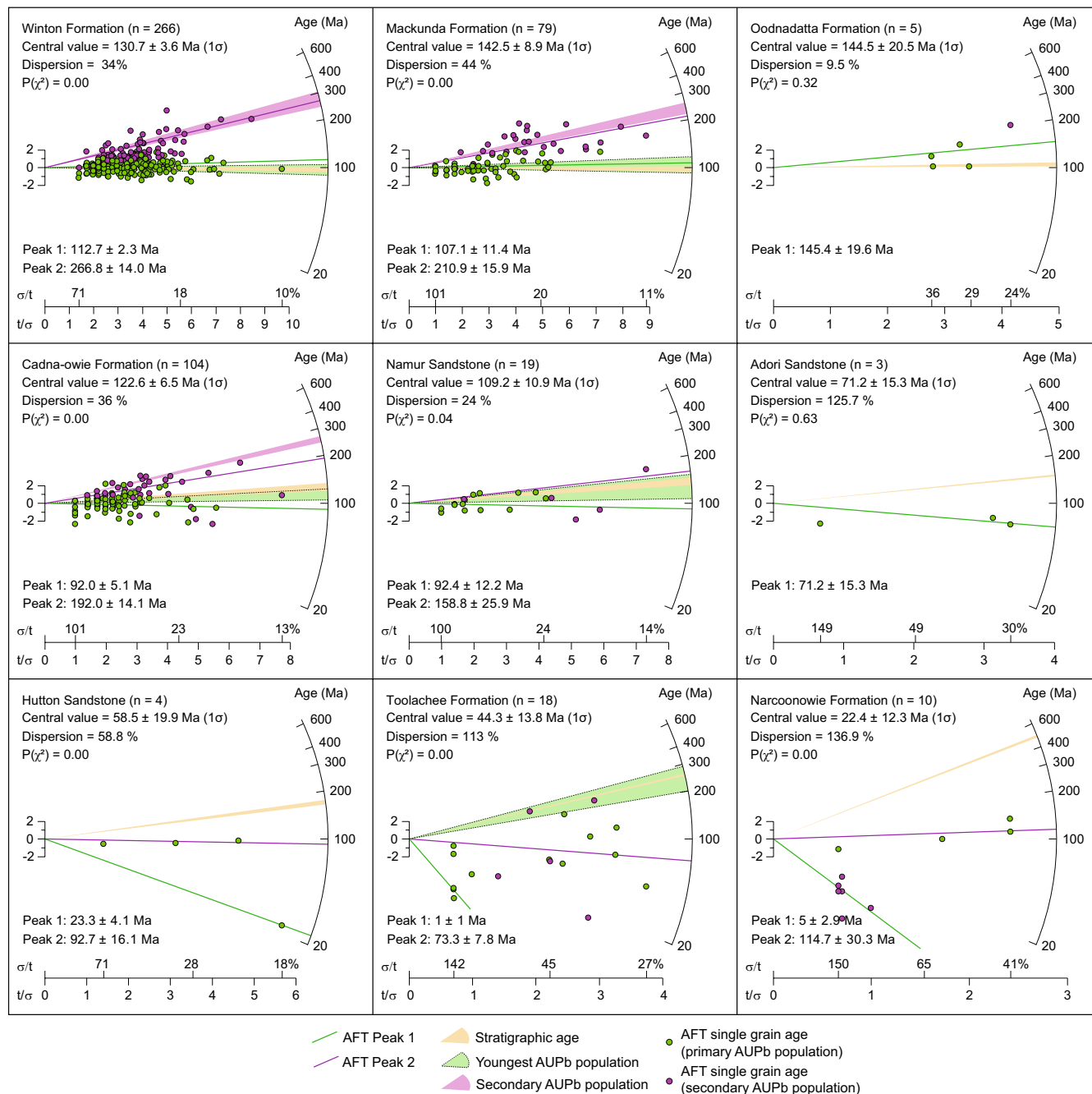


**FIGURE 4** AFT radial plots grouped for each sampled formation. Individual grains are coloured corresponding with primary and secondary age populations shown in Figure 3, determined by a combination U–Pb ratio and single-grain AFT age. Grains are attributed to the primary population by default, with apatites only ascribed to the secondary population if they deviate significantly from the youngest AUPb isochron and/or AFT peak. Where applicable, corresponding pooled AUPb population ages for each formation have been provided, as has the stratigraphic age of the sampled unit.

in each analytical session (Vermeesch, 2017). Weighted mean AFT ages for Durango apatite of  $30.2 \pm 1.7$  Ma (session LA-2017),  $29.1 \pm 3.5$  Ma (session LA-2018a) and  $28.3 \pm 4.5$  Ma (session LA-2018b) are within uncertainty of the published standard AFT age of  $31.7 \pm 2.1$  Ma (Cogné et al., 2020) and  $^{40}\text{Ar}/^{39}\text{Ar}$  age of  $31.44 \pm 0.18$  Ma (McDowell et al., 2005) for Durango apatite, suggesting fission track ages produced in these sessions are reliable.

#### 4.2.2 | Radial plots

The following section describes AFT results as provided from the radial plots in Figure 4. AFT data from the Eromanga Basin commonly exhibit open-jaw characteristics and fail the chi-square test (Figure 4; Table 3), indicative of multiple age populations preserved within single samples (O'Sullivan & Parrish, 1995; Vermeesch, 2017).

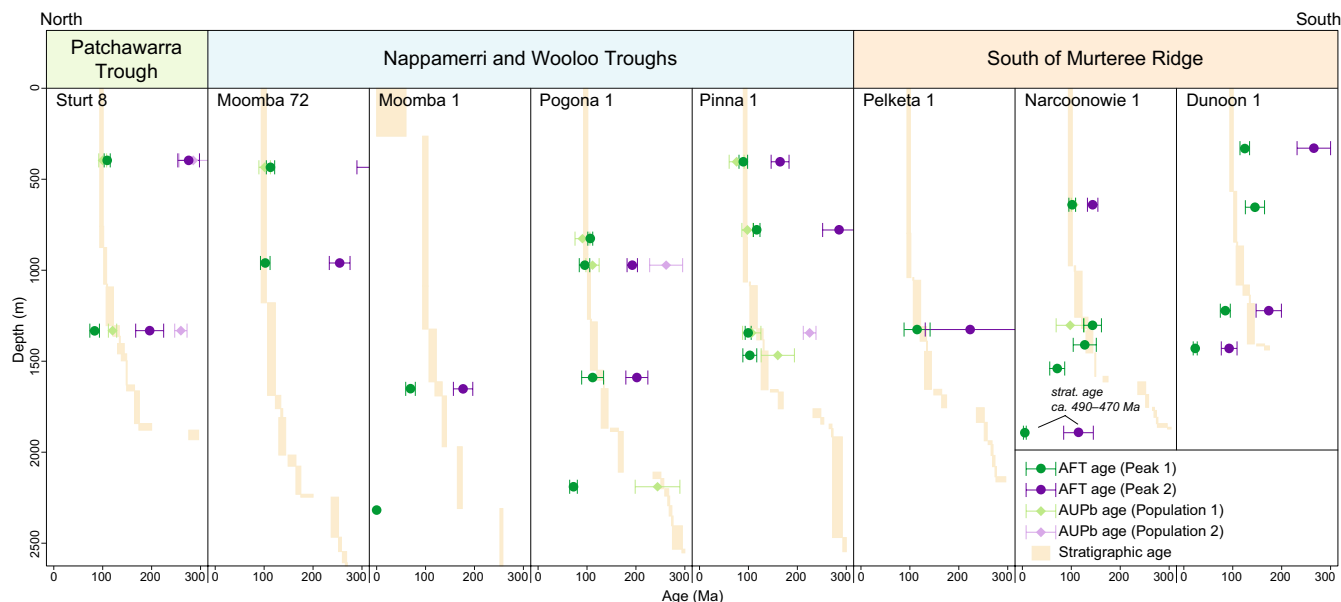


**FIGURE 5** Summary of AFT and AUPb ages across the Cooper–Eromanga Basin, showing progression of down-hole ages and associated stratigraphic ages.

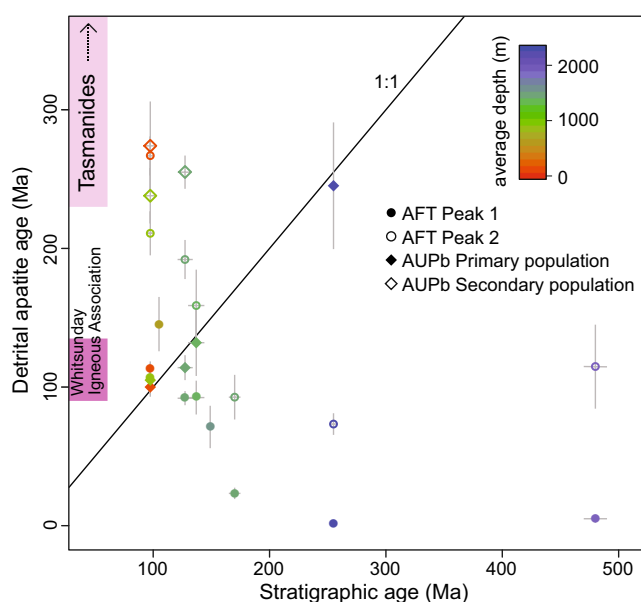


**FIGURE 6** Comparison of pooled formation AUPb and AFT ages with stratigraphic ages. Ages are coloured by average sample depth.

For such samples, multiple age peaks were successfully calculated, using IsoplotR software (Vermeesch, 2018). Additionally, individual grains in radial plots were colour coded in accordance with the AUPb age peak to which they were assigned (green for grains in the primary AUPb populations, and purple for grains in the older AUPb populations), or subjectively by AFT peak if samples demonstrate open-jaw characteristics in radial plot space (see Appendix S1 for full rationale). This strategy allowed

validation of the AFT populations and cross-calibration of AFT and AUPb populations for provenance analysis.

Six samples from the Winton Formation (ca. 101–94 Ma) between depths of 1006–283 m yielded a pooled population which displays open-jaw characteristics and fails the chi-squared test ( $\chi^2=0.00$ ). Peak AFT ages at  $113 \pm 2$  Ma and  $267 \pm 14$  Ma are consistent with AUPb population ages for this formation (Figure 4). Similarly, two pooled samples from the Mackunda Formation (ca. 102–94 Ma) taken between depths of 1006–747 m fail the chi-square test ( $\chi^2=0.00$ ) and yield peak ages at  $107 \pm 11$  Ma and  $211 \pm 16$  Ma, which are within uncertainty of AUPb population ages within this formation (Figure 4). The youngest AFT age peaks for both the Winton Formation and Mackunda Formation are within uncertainty of the stratigraphic age of these formations. A single sample from the Oodnadatta Formation (Du1-2) sampled at 686–622 m passes the chi-squared test ( $\chi^2=0.32$ ) and yields an AFT central age of  $145 \pm 21$  Ma, which is older than the stratigraphic age of this formation (ca. 108–102 Ma). AFT age peaks consistent with or older than stratigraphic ages within these formations suggest AFT data from these samples retain provenance information and have not been significantly thermally reset post-deposition.

Six samples taken from the Cadna-owie Formation (ca. 134–121 Ma) between depths of 1685–1284 m returned a pooled population which fails the chi-square test ( $\chi^2=0.00$ ). Two peak AFT ages at  $92 \pm 5$  Ma and  $192 \pm 14$  Ma are slightly younger than the respective AUPb age populations reported for this population (Figure 4). The pooled population of three samples from the Namur Sandstone (ca. 144–130 Ma) sampled between depths of 1484–1207 m

**TABLE 3** Summary of AFT results for individual samples.  $\rho_s$  represents the average surface density of spontaneous fission tracks.  $N_s$  is the total number of spontaneous fission tracks counted in the sample.  $n$  is the number of grains analysed in the sample.  $U$  is the average concentration of uranium for all grains in the sample, with uncertainty given as two standard deviations. Central Age is the sample AFT central age as calculated using IsoplotR software (Vermeesch, 2018), while peak ages have additionally been calculated for samples displaying open-jaw characteristics. All age errors represent  $1\sigma$ .  $P(\chi^2)$  is the chi-square probability that all grains in the population may be attributed to a single-age population. MTL is the mean confined track length, with uncertainty quoted as one standard deviation.  $n_i$  is the number of confined tracks measured for all grains of the sample. Stratigraphic ages based on framework of Gravestock et al. (1998), Hall et al. (2015, 2019), Bradshaw et al. (2022) and Hannaford et al. (2022). Individual radial plots are provided in Appendix S1.

Sample	Unit	Stratigraphic		Central age					$n$	Peak 1 (Ma)	Peak 2 (Ma)	MTL ( $\mu\text{m}$ )	$n_t$
		age (Ma)	$\rho_s$ ( $\times 10^7/\text{cm}^2$ )	$N_s$	U (ppm)	(Ma)	$p$ ( $\chi^2$ )						
Dul-1	Winton Formation	ca. 101-94	5.05	281	8.2 $\pm$ 10.4	141.5 $\pm$ 12.5	0	19	124.7 $\pm$ 9.1	265.9 $\pm$ 35.8	13.4 $\pm$ 1.6	30	
St8-1	Winton Formation	ca. 101-94	5.06	651	6.6 $\pm$ 13.7	148 $\pm$ 12.9	0	38	109.2 $\pm$ 6.2	275.7 $\pm$ 22.1	12.1 $\pm$ 1.8	22	
Pil-1	Winton Formation	ca. 101-94	2.39	563	4.4 $\pm$ 4.8	115.4 $\pm$ 7.5	0	45	93.5 $\pm$ 8.8	168.7 $\pm$ 18.3	12.7 $\pm$ 1.7	68	
M72-1	Winton Formation	ca. 101-94	3.81	356	5.7 $\pm$ 10.8	160.1 $\pm$ 19.9	0	23	113.0 $\pm$ 8.5	345.6 $\pm$ 55.9	11.9 $\pm$ 2.1	59	
Na1-1	Winton Formation	ca. 101-94	3.53	1434	6.3 $\pm$ 11.4	120.4 $\pm$ 3.9	0.07	96	101.7 $\pm$ 7.0	143.6 $\pm$ 10.7	13.5 $\pm$ 1.5	62	
Po1-1	Winton Formation	ca. 101-94	3.52	636	6.6 $\pm$ 9.5	122.2 $\pm$ 10.7	0	32	108.8 $\pm$ 4.8	484.4 $\pm$ 84.2	12.1 $\pm$ 1.8	38	
M72-2	Winton Formation	ca. 101-94	3.80	390	4.6 $\pm$ 4.2	172.2 $\pm$ 22.6	0	13	102.3 $\pm$ 9.8	254.4 $\pm$ 21.2	11.2 $\pm$ 2.1	21	
Pil-2	Mackunda Formation	ca. 102-94	4.20	719	6.2 $\pm$ 9.5	140.9 $\pm$ 11.1	0	50	120.9 $\pm$ 6.7	289.3 $\pm$ 33.6	12.8 $\pm$ 1.5	38	
Po1-2	Mackunda Formation	ca. 102-94	4.76	655	6.3 $\pm$ 9.7	145.5 $\pm$ 14.9	0	29	95.9 $\pm$ 10.7	193.5 $\pm$ 10.6	12.2 $\pm$ 2.2	21	
Dul-2	Oodnadatta Formation	ca. 108-102	3.26	57	4.7 $\pm$ 2.5	144.5 $\pm$ 20.5	0.32	5	145.4 $\pm$ 19.6	—	—	—	
Na1-2	Cadna-owie Formation	ca. 134-121	2.85	64	4.0 $\pm$ 3.9	143.4 $\pm$ 18.2	0.68	11	143.4 $\pm$ 18.2	—	—	—	
Pe1-1	Cadna-owie Formation	ca. 134-121	2.39	44	4.0 $\pm$ 3.9	136.7 $\pm$ 23.6	0.38	9	114.7 $\pm$ 26.6	227.1 $\pm$ 95.7	—	—	
St8-2	Cadna-owie Formation	ca. 134-121	4.37	188	16.3 $\pm$ 79.1	127.4 $\pm$ 15.1	0	22	83.5 $\pm$ 9.8	196.0 $\pm$ 28.6	—	—	
Pil-3	Cadna-owie Formation	ca. 134-121	3.81	317	8.4 $\pm$ 24.1	101.0 $\pm$ 8.8	0.01	30	103.5 $\pm$ 6.1	—	—	—	
Po1-3	Cadna-owie Formation	ca. 134-121	2.43	173	3.0 $\pm$ 3.4	161.4 $\pm$ 17.1	0.10	15	112.5 $\pm$ 22.4	202.9 $\pm$ 22.5	—	—	
M1-1	Cadna-owie Formation	ca. 134-121	2.50	176	6.0 $\pm$ 15.7	118.8 $\pm$ 18.3	0	17	69.2 $\pm$ 9.8	176.7 $\pm$ 19.8	13.1 $\pm$ 1.7	22	
Dul-4	Namur Sandstone	ca. 144-130	13.67	148	26.1 $\pm$ 19.9	106.6 $\pm$ 20.1	0	4	84.8 $\pm$ 10.2	173.6 $\pm$ 25.9	10.5 $\pm$ 1.2	37	
Na1-3	Namur Sandstone	ca. 144-130	6.12	31	9.9 $\pm$ 2.5	127.5 $\pm$ 23.6	0.53	2	127.5 $\pm$ 23.6	—	—	—	
Pil-4	Namur Sandstone	ca. 144-130	2.25	58	4.9 $\pm$ 5.8	106.8 $\pm$ 14.2	0.73	13	106.8 $\pm$ 14.2	—	—	—	
Na1-4	Adori Sandstone	ca. 150-148	3.91	22	10.3 $\pm$ 9.6	71.2 $\pm$ 15.3	0.63	3	71.2 $\pm$ 15.3	—	—	—	
Dul-6	Hutton Sandstone	ca. 175-165	6.28	72	28.9 $\pm$ 58.6	58.5 $\pm$ 19.9	0	4	23.3 $\pm$ 4.1	92.7 $\pm$ 16.1	—	—	
Po1-6	Toolachee Formation	ca. 258-252	2.44	94	7.8 $\pm$ 9.8	68.4 $\pm$ 15.6	0	15	73.4 $\pm$ 7.8	—	—	—	
M1-5	Toolachee Formation	ca. 258-252	0	0	59.6 $\pm$ 50.4	0	—	—	—	—	—	—	
Na1-6	Narconowie Formation	ca. 480-470	0.75	16	10.1 $\pm$ 17.6	22.4 $\pm$ 12.3	0	10	5.0 $\pm$ 2.9	114.7 $\pm$ 30.3	—	—	



similarly fail the chi-square test ( $\chi^2=0.04$ ). The youngest peak AFT age for this population at  $92\pm 12$  Ma is notably younger than the complementary AUPb age population (ca.  $123\pm 24$  Ma; Figure 4), while no secondary AUPb age was able to be calculated to compare to the older AFT peak age of  $159\pm 26$  Ma. The youngest AFT peak ages for both the Cadna-owie Formation and Namur Sandstone are younger than the stratigraphic ages of the respective units, while the oldest peak ages are older than the stratigraphic ages, which is suggestive of partial thermal resetting of the AFT system in these populations.

A single sample (Du1-6) from the Hutton Sandstone (ca. 175–165 Ma) sampled at 1442–1417 m fails the chi-square test ( $\chi^2=0.00$ ), and yields an AFT central age of  $59\pm 20$  Ma and potential peak ages at  $23\pm 4$  Ma and  $93\pm 16$  Ma. All these age peaks are notably younger than the stratigraphic age of this unit (Figure 4). A single sample (Na1-4) from the Adori Sandstone (ca. 150–148 Ma) obtained from a depth of 1583–1497 m passes the chi-square test ( $\chi^2=0.63$ ) and preserves an AFT central age of  $71\pm 15$  Ma, which is notably younger than the stratigraphic age (Figure 4). AFT age peaks from both the Hutton Sandstone and Adori Sandstone are consistently younger than the depositional ages of the respective formations, suggesting AFT ages within these samples have been thermally reset after deposition.

Two samples have been analysed from the Toolachee Formation (ca. 258–252 Ma) in the Cooper Basin, collected between depths of 2318–2149 m. The pooled AFT population for the Toolachee Formation displays very high dispersion (113%) and fails the chi-square test ( $\chi^2=0.00$ ), despite not displaying open-jaw characteristics. A central age at  $44\pm 14$  Ma is significantly younger than the stratigraphic age of the Toolachee Formation and AUPb age obtained for this formation ( $245\pm 46$  Ma; Figure 4), although some single grains do lie within error of the stratigraphic age. A single sample (Na1-4) from the Narcoonowie Formation (ca. 480–470 Ma; Gravestock et al., 1998) of the Warburton Basin obtained from a depth of 1887–1871 m similarly fails the chi-square test ( $\chi^2=0.00$ ) due to its high dispersion (137%). Similar to that observed in the Toolachee Formation, AFT age peaks in this sample at  $5\pm 3$  Ma and  $115\pm 30$  Ma and a central age of  $22\pm 12$  Ma are considerably younger than the stratigraphic age, suggesting AFT samples within the Toolachee Formation and Narcoonowie Formation experienced significant thermal resetting following deposition within the respective basins.

#### 4.2.3 | Thermal history modelling

Thermal history reconstructions were conducted using a consistent modelling approach for all samples in a given

well, and produced some spatial variation across the basin (Figure 7). Modelled wells within the Nappamerri Trough, north of the Murteree Ridge (Moomba 1 and 72, Pogona 1, Pinna 1 and Sturt 8), all suggest heating during the Late-Cretaceous at ca. 95–75 Ma, following deposition of the Winton Formation. Of these wells, Moomba 1, Moomba 72, Pinna 1 and Sturt 8 predict a subsequent cooling phase from ca. 75 to 40 Ma, while thermal modelling for Pogona 1 predicts a continued steady rise in temperatures. South of the Murteree Ridge, wells Dunoon 1 and Narcoonowie 1 predict mild heating during progressive deposition in the Eromanga Basin until the end of sedimentation in the Winton Formation at ca. 94 Ma, but do not display the Cretaceous thermal perturbations observed north of the structure. In the northeast of the study area, thermal history models for wells Moomba 1, Moomba 72, Pinna 1 and Narcoonowie 1 suggest a significant additional recent reheating event since ca. 30 Ma, which appears absent in other wells. AFT data are not considered sufficient to confidently infer palaeogeothermal gradients, hence discussion is confined to timing and relative magnitudes of predicted thermal events.

## 5 | DISCUSSION

### 5.1 | Provenance

#### 5.1.1 | Upper Eromanga Basin (Winton, Mackunda and Cadna-owie Formations)

##### 5.1.1.1 | Primary (Cretaceous) Provenance

Deposition in the upper Eromanga Basin from the Cadna-owie Formation to Winton Formation occurred between ca. 134 and 94 Ma, in an evolving marine and fluvial environment (Alexander & Hibburt, 1996; Veevers et al., 1991). The Cadna-owie Formation (ca. 134–121 Ma) was deposited at the transition between the Eromanga Sea and terrestrial environments (Alexander & Hibburt, 1996). As marine transgression progressed, the entirety of the Eromanga Basin became submerged by ca. 118 Ma (Figure 8), facilitating deposition of marine units such as the ca. 102–94 Ma Mackunda Formation (Veevers et al., 1991). During the Late-Cretaceous, marine regression of the Eromanga Sea facilitated depositional regime transition to a large west-flowing fluvial system, in which the Winton Formation (ca. 101–94 Ma) was deposited. Despite these variations in depositional environments, the primary (Cretaceous) AUPb and AFT ages for all upper Eromanga Basin formations obtained in this study were comparable to the stratigraphic age for each respective unit (Figures 4–6).

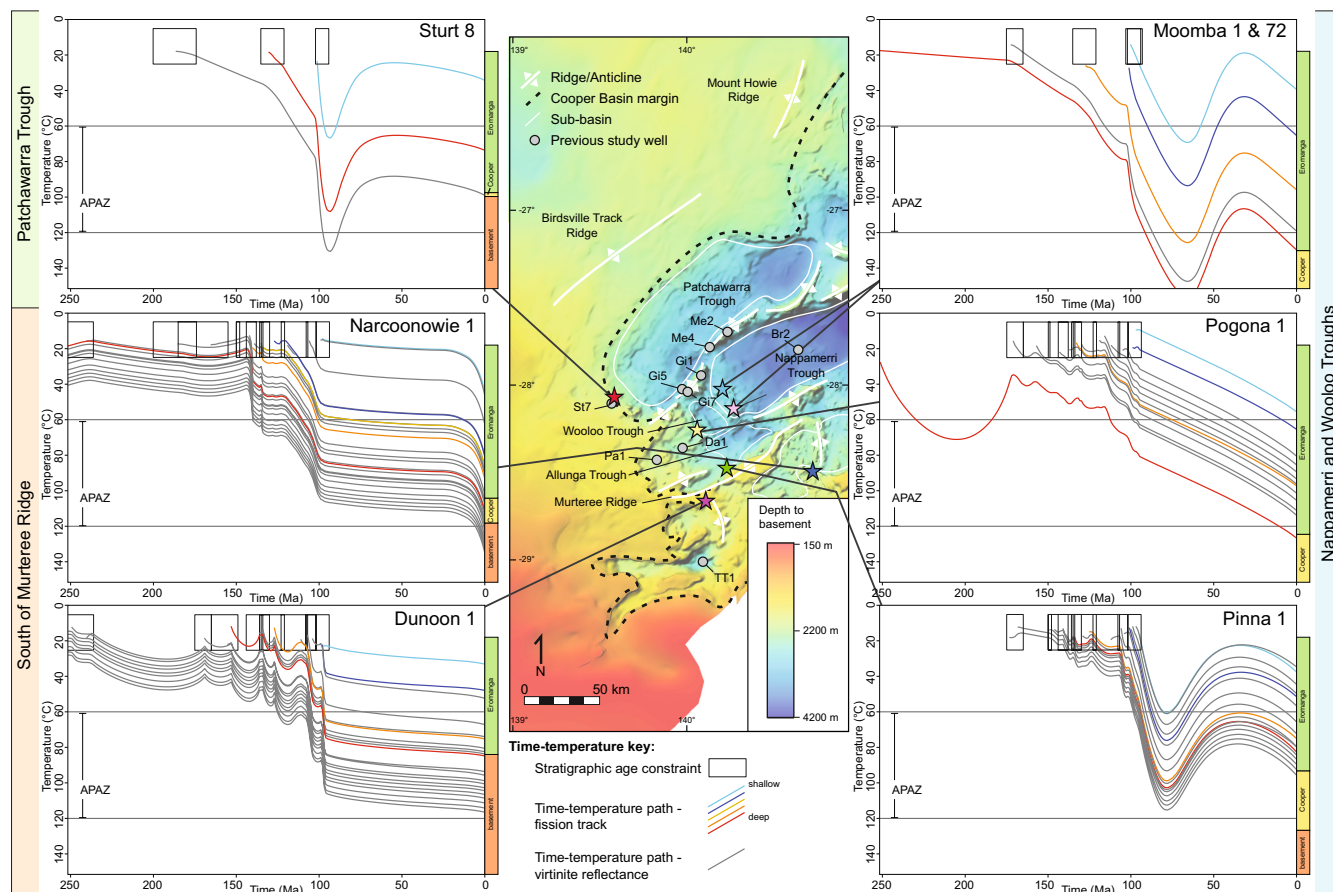


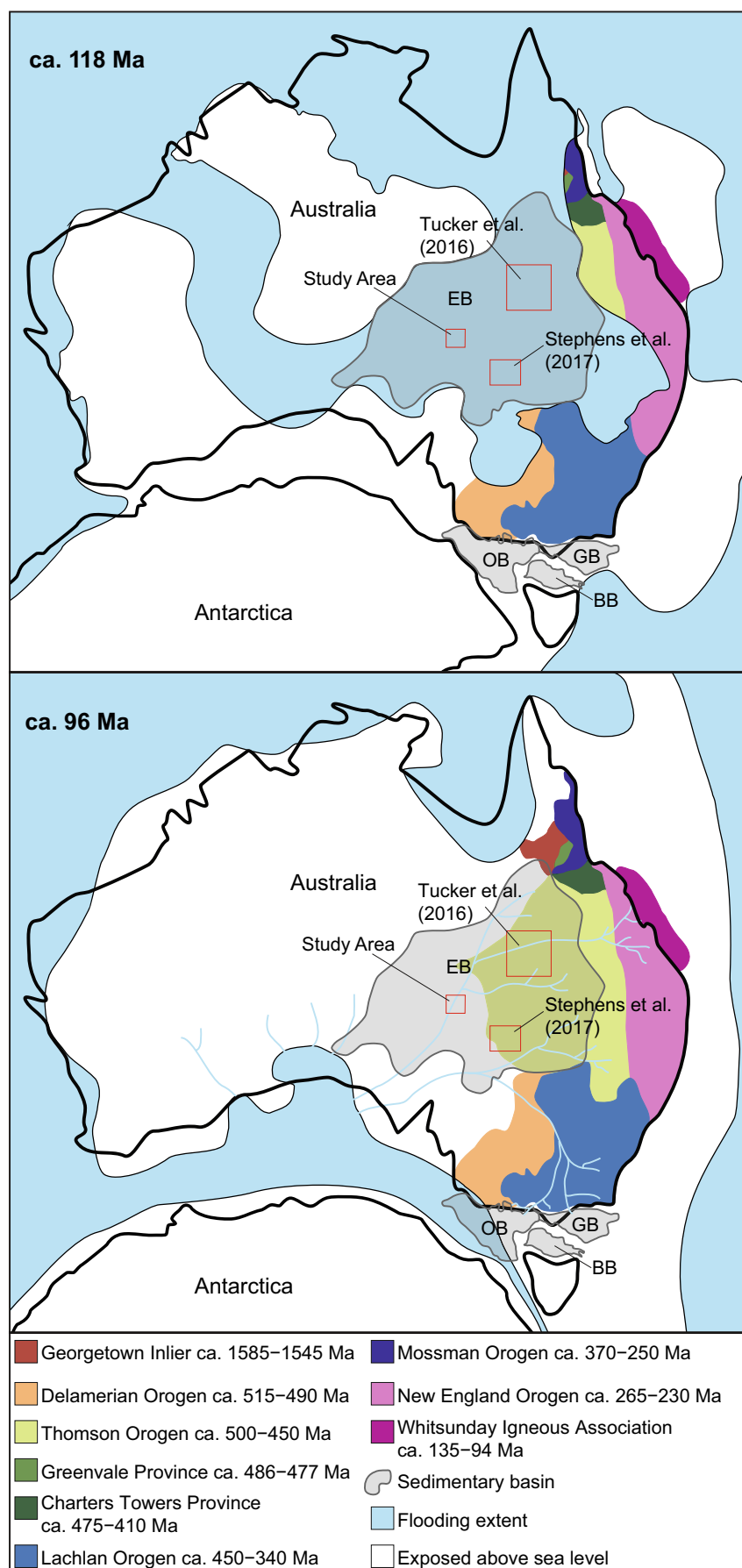
**FIGURE 7** Time-temperature models for the Sturt 8, Pogona 1, Dunoon 1, Pinna 1, Narcoonowie 1 and combined Moomba 1 and Moomba 72 wells, shown by location within the Cooper-Eromanga Basin. The apatite partial annealing zone (APAZ) is the thermal range at which fission tracks in apatite sensitive over geological time scales (ca. 120–60°C; Gleadow et al., 1986; Wagner & Van den haute, 1992), and has been indicated for each reconstruction. Present day stratigraphic levels of the Eromanga Basin, Cooper Basin and pre-Permian basement are shown to the right of each thermal history profile. Wells previously studied for thermal history and referenced from Duddy and Moore (1999) and Duddy et al. (2002) are additionally shown, with well names as follows: Bu2, Burley 2; Da1, Daralingie 1; Gi1, Gidgelpa 1; Gi5, Gidgelpa 5; Gi7, Gidgelpa 7; Me2, Merrimelia 2; Me4, Merrimelia 4; Pa1, Pando 1; St7, Sturt 7; TT1, Tinga Tingana 1.

Primary AUPb age populations from the upper Eromanga Basin (Winton Formation:  $100 \pm 5$  Ma; Mackunda Formation:  $105 \pm 12$  Ma) are comparable with detrital zircon age peaks in equivalent strata from the Eromanga Basin observed in northeast Queensland (Figure 8; Tucker et al., 2016). Multiple ZUPb age peaks have been picked in the sequential Mackunda and Winton Formations at ca. 111, 105, 99 and 95 Ma in the eastern Eromanga Basin (Tucker et al., 2016), with individual age peaks interpreted as pulses of volcanism within the Whitsunday Igneous Association. An older zircon peak detected within these strata at ca. 121 Ma (Tucker et al., 2016) is consistent with that observed in the AUPb record of the Cadna-owie Formation at  $114 \pm 9$  Ma (Figure 3), is also interpreted to have been sourced from Whitsunday volcanism. While precision of AUPb analysis is not sufficient to isolate individual volcanic pulses as preserved within the zircon record, the observed similarities between primary AUPb ages, youngest ZUPb ages and stratigraphic ages suggest that the Cretaceous upper Eromanga Basin

apatites were largely sourced from a single, syn-depositional source as suggested by Veevers (1984). Cretaceous apatites were most likely sourced from ca. 135 to 90 Ma volcanism in the Whitsunday Igneous Association (Bryan et al., 2000; Ewart et al., 1992) in northeastern Australia, as proposed by Tucker et al. (2016). Detritus from this distal source was likely transported in marine, and later fluvial environments (Bryan et al., 2000), or as fallout from explosive eruptions carried by easterly polar winds (Barham et al., 2016).

The Whitsunday Igneous Association was also a major sediment source for the Otway, Gippsland and Bass Basins (Figure 8; Bryan et al., 1997; Norvick, 2005), while zircons attributed to this terrane have been observed as far southwest as the Ceduna Delta (Lloyd et al., 2016; MacDonald et al., 2013). During deposition of the Winton Formation in the middle Cretaceous these basins were uplifted as a response to large-scale platform tilt at the east Australian margin, with up to 3 km of sedimentary material eroded from ca. 103 Ma into the Late-Cretaceous (Röth, 2022).

**FIGURE 8** Key source terranes for the Eromanga Basin in the middle Cretaceous, and relationship to evolving depositional environments from the Aptian–Cenomanian. Marine inundation of Australia was greatest in the Aptian and Albian (including deposition of the Mackunda Formation), before sea level receded and transitioned to a fluvial environment (facilitating deposition of the Winton Formation). The area of this study has been indicated along with detrital zircon studies of Tucker et al. (2016) and Stephens et al. (2017). Compiled using elements of Bryan et al. (2012), Cawood et al. (2011), Fergusson and Henderson (2015), Fergusson et al. (2005), Foden et al. (2006), Tucker et al. (2016) and Veevers et al. (1991). Basin names are as follows: EB, Eromanga Basin; GB, Gippsland Basin; BB, Bass Basin; OB, Otway Basin.



Considerable detritus from these uplifted basins was transported in westward flowing fluvial systems and quickly redeposited in the Winton Formation of the Eromanga Basin (Figure 8). These fluvial systems likely transported Early-Cretaceous detritus from the Otway, Gippsland and Bass Basins into the Eromanga Basin during this time (Röth, 2022), but additionally syn-sedimentary volcanogenic material from the Whitsunday Igneous Association.

It remains unclear whether the Whitsunday Igneous Association was actually responsible for large volumes of detritus deposited within the Eromanga Basin, or is disproportionately represented in the age record due to the prevalence of volcanic apatites and zircons sourced from eruptions. If a significant amount of sediment was sourced from the Whitsunday Igneous Association, it is likely that the terrane was once more extensive than observed today, with much of the original terrane now submerged off the east coast of Australia (Bryan et al., 1997). Alternatively, MacDonald et al. (2013) suggested that middle Cretaceous volcanogenic sediments within the Ceduna Delta were sourced from easily eroded inland local volcanic centres which have not been preserved. While Mesozoic volcanism has been observed proximally in the eastern Cooper Basin (Hardman et al., 2019; Röth & Littke, 2022), there are no currently identified pulses of activity which correspond with deposition throughout the upper Eromanga Basin sequences, hence the more established Whitsunday Igneous Association is considered a more likely source.

#### 5.1.1.2 | Secondary (Permian–Triassic) Provenance

Secondary AUPb populations within the Winton Formation, Mackunda Formation and Cadna-owie Formation cluster between ca. 280 and 230 Ma, and are quite consistent across formations (Table 2). These AUPb ages are further comparable to a previously identified Permian age peak in detrital ZUPb ages from the upper Eromanga Basin (Tucker et al., 2016). Secondary AFT age populations showed more variation (Figures 4 and 5), however, shallow basin samples (<1000 m) are consistent with observed AUPb populations of respective units. AFT secondary ages from the Winton Formation and Mackunda Formation preserve secondary AFT ages within error of respective secondary AUPb ages between ca. 280 and 230 Ma (Figure 6), and hence likely retain provenance information. The Cadna-owie Formation preserves a secondary AFT peak at  $192 \pm 14$  Ma, which is younger than the population secondary AUPb age (Figures 4 and 6), hence it is likely that these deeper samples (>1280 m) have been partially thermally reset and thus no provenance information can be gleaned from these AFT data. These older age populations suggest that ca. 280–230 Ma detritus in the upper Eromanga Basin was sourced from Carboniferous–Triassic provenances. The most likely source terranes are located in the nearby Tasmanide

orogens of eastern Australia (e.g. Cawood et al., 2011; Fergusson & Henderson, 2015; Quentin de Gromard, 2013; Rosenbaum, 2018; Tucker et al., 2016), with detritus shed from uplifted regions and transported in a combination of marine and fluvial systems (Figure 8).

### 5.1.2 | Lower Eromanga Basin (Namur Sandstone)

#### 5.1.2.1 | Primary (Cretaceous) Provenance

The Namur Sandstone was deposited in a fluvial environment in a north-flowing river system at ca. 144–130 Ma (Alexander & Hibbert, 1996). A primary AUPb age population is observed in this formation at  $123 \pm 24$  Ma which is within error of the documented stratigraphic age. AFT ages from the Namur Sandstone have been thermally reset following deposition (Figures 4–6), thus yield no provenance information. While AUPb ages from the Namur Sandstone are associated with large uncertainties, these ages do suggest a syn-depositional sediment source. Syn-depositionally sourced apatites in younger formations have been attributed to the Whitsunday Igneous Association, and the onset of volcanism in this suite at ca. 135 Ma (Bryan et al., 2012) did begin prior to the minimum depositional age of the Namur Sandstone. Contemporaneous volcanism was additionally active outboard from the eastern Australian margin prior to initiation in the Whitsunday Igneous Association, during development of the Tasmanides (e.g. Crook, 1980; Henderson et al., 2011) and through the entire depositional window of the Namur Sandstone, and thus provides another plausible candidate for apatite provenance. Comparable sediments are observed in the Otway, Gippsland, Bass and Surat Basins (e.g. Norvick, 2005; Röth et al., 2022; Sircombe, 1999), and such a volcanic system would appear to be the only recognised Cretaceous syn-depositional source prior to the onset of volcanism in the Whitsunday Igneous Association.

Cretaceous AUPb ages obtained from this study contrast strongly with ZUPb ages presented by Stephens et al. (2017), who proposed a dominant Cambrian to Mesoproterozoic source for the Namur Sandstone in eastern Australia. The observed discrepancy likely reflects localised variations in sediment provenance, as sediment in the Eromanga Basin in eastern Australia was sourced from diverse basement outcrops (Stephens et al., 2017), whereas apatites from this study in central Australia reflect a more distal source. Distal volcanism during subduction at the eastern margin resulted in extrusion of dominantly mafic suites (Crook, 1980; Henderson et al., 2011). Given that apatite is more abundant than zircon in mafic rocks, where zircon can be entirely absent (Chew et al., 2020), it



is more likely for apatites to appear in the detrital record compared to zircons.

### 5.1.3 | Upper Cooper Basin (Toolachee Formation)

#### 5.1.3.1 | Primary (Carboniferous–Permian)

##### *Provenance*

Deposition of the Toolachee Formation in the Cooper Basin occurred in fluvial to lacustrine environments at ca. 258–252 Ma (Drexel & Preiss, 1995; Gravestock et al., 1998; Hall et al., 2015, 2019). The single AUPb age peak identified at  $245 \pm 46$  Ma is within error of stratigraphic age, but potentially comprises multiple age populations that are unable to be distinguished due to the low number of available grains. AFT ages were partially reset after deposition, thus do not preserve provenance information (Figures 4–6). The observed AUPb ages are consistent with a distal sediment provenance (Figure 8) from the Mossman (ca. 370–250 Ma; Black et al., 2005; Rosenbaum, 2018) and New England orogenic belts (ca. 265–230 Ma; Collins, 1991; Roberts & Engel, 1987; Rosenbaum et al., 2012; Rosenbaum, 2018). These terranes have further been proposed as sources for sediment within subsequent Eromanga Basin strata (Allen et al., 1998; Quentin de Gromard, 2013), which suggests a continued source of sediment from eastern Australia to the Cooper–Eromanga Basin from the late-Permian into the Cretaceous.

## 5.2 | Thermal history

### 5.2.1 | Cretaceous heating pulse

Thermal history models from all wells north of the Murteree Ridge suggest steady post-depositional heating of sediments since ca. 100 Ma, with prevailing high temperatures through ca. 90–70 Ma (Figure 7). The timing of the heating pulse is consistent with results presented by Duddy et al. (2002) and Röth and Littke (2022), who predict a thermal maximum at ca. 100–70 Ma. Variations in timing of thermal maxima are largely attributed to modelling uncertainty and differing quality of apatite data between individual wells. The magnitude of Cretaceous peak temperatures correlates with basement depth, and likely reflects the total burial depth. Wells south of the Murteree Ridge (Narcoonowie 1 and Dunoon 1) exhibit post-depositional heating, but show no evidence for subsequent Late-Cretaceous cooling (Figure 7). Temperatures in westernmost wells (Dunoon 1 and Sturt 8) appear to have remained relatively stable since the deposition of the Winton Formation (ca. 101–94 Ma) until the Cenozoic.

As the duration of Cretaceous heating coincided with progressive burial in the Eromanga Basin (Alexander & Hibburt, 1996; Duddy et al., 2002; Röth & Littke, 2022), consideration must be given to whether this thermal maximum was reached by rapid subsidence and associated sedimentary burial alone, or if additional heat sources would have been required. Rapid subsidence in central Australia and corresponding high eustatic sea levels between ca. 120 and 90 Ma (Braz et al., 2021; Gurnis et al., 1998) coincide with the timing of deposition of thick sedimentary sequences in the Eromanga Basin (Alexander & Hibburt, 1996; Röth & Littke, 2022). More significantly, the Cooper–Eromanga Basin experienced considerable episodic magmatic and hydrothermal activity throughout the Mesozoic, causing considerable subsurface thermal perturbations (e.g. Gallagher, 1988; Hardman et al., 2019; McLaren & Dunlap, 2006; Röth, 2022; Röth & Littke, 2022). Renewed hydrothermal circulation in the Late-Cretaceous, therefore, appears a likely driver of the observed thermal peak at ca. 95–70 Ma, enhanced by local magmatism or basal heat flow contributions (Hardman et al., 2019; Röth & Littke, 2022).

Duddy et al. (2002) predicted very high geothermal gradients in the middle Cretaceous of ca. 80–75 °C/km, while more recent estimates by Röth and Littke (2022) suggest a maximum gradient of ca. 74 °C/km. Both estimates are considerably higher than the present-day geothermal gradients which reach ca. 60 °C/km, and are consistent with high heat flow regimes expected in a rift environment, and suggest a possible middle Cretaceous aborted rift below the basin. Importantly, however, no middle Cretaceous thermal pulse has been observed in wells south of the Murteree Ridge in this study, while previous thermal history modelling of the Tinga Tingana 1 well similarly yields little evidence for such a pulse (Figure 7; Gravestock et al., 1998). This disparity indicates considerable segmentation of the basin thermal structure, which is more indicative of a more localised basal heat source. Episodic volcanism in the so-called ‘Cooper Hot Spot’, a mafic volcanic province which intrudes the Nappamerri Trough (Figures 1 and 7) and was sporadically active throughout the Mesozoic (Hardman et al., 2019; Röth & Littke, 2022) presents as an alternate candidate for magmatic activity coincident with the middle Cretaceous heating pulse. It appears most plausible that hydrothermal circulation linked to activity reactivation of the Cooper Hot Spot was responsible for the observed thermal peaks at ca. 95–70 Ma north of the Murteree Ridge (Figure 7), while fluids from this northern source were largely unable to infiltrate south of the structure. The Pogona 1 well on the flank of the Wooloo Trough (Figure 7) similarly does not record a sharp middle Cretaceous heating pulse, suggesting this well also may have been largely unaffected by this hydrothermal circulation.

## 5.2.2 | Late-Cretaceous cooling phase

Cooling in the Eromanga Basin after the Cretaceous thermal maximum has previously been attributed to a period of exhumation, hydrological processes and basal heat flow relaxation (Deighton & Hill, 1998; Röth & Littke, 2022). In the Late-Cretaceous, sedimentation in the Eromanga Basin ceased as the basin became fully subaerially exposed (Alexander & Hibbert, 1996). Uplift in the Eromanga Basin in the Late-Cretaceous coincided with uplift on the eastern Australia margin, as westward motion of the Pacific plate increased and the plate rotated clockwise to shift from normal to sinistral subduction below the eastern margin of Australia (Veevers, 2000). Additional factors of isostatic rebound in central Australia, continental platform tilt, eustatic sea level and dynamic mantle-induced topography may have further contributed to Cretaceous uplift in eastern and central Australia (Braz et al., 2021; Bryan et al., 2012; Gurnis et al., 1998; Röth, 2022) facilitating erosion approaching 1 km between ca. 80 and 60 Ma in parts of the Eromanga Basin (Braz et al., 2021; Röth & Littke, 2022).

Thermal models throughout the Cooper–Eromanga Basin differ slightly with regards to the maximum temperatures experienced, and the timing and magnitude of subsequent cooling. North of the Murteree Ridge, the combined Moomba 1 and Moomba 72 wells located within the basin centre and the Pinna 1 well closer to the Murteree Ridge exhibit cooling in the Cadna-owie Formation from ca. 130 to 90°C, respectively, at ca. 75–50 Ma (Figure 7). Sturt 8 well located at the Cooper Basin margin exhibit cooling from ca. 120°C slightly earlier at ca. 90–60 Ma. In both cases, it is probable that predicted cooling during the Late-Cretaceous was facilitated by a combination of exhumation coinciding with fading activity of the Cooper Hot Spot and associated hydrothermal circulation.

Seismic analysis conducted by Kulikowski and Amrouch (2018) suggests that the Cooper–Eromanga basin experienced significant structural reactivation during the Late-Cretaceous to early Cenozoic during a period of compression (Mavromatidis, 2008). Notably, the final period of fault activity between ca. 95 and 65 Ma was responsible for a regional unconformity between Late-Cretaceous and Palaeogene sediments and corresponds with the timing of cooling within the basin (Figure 7). Significant folding and sediment thickening and the presence of inversion structures through the Nappamerri Trough suggest that the widespread tilting due to compression was partly responsible for the greater extent of exhumation and cooling within the trough and north of the Murteree Ridge, relative to wells located at the basin margins (Mavromatidis, 2008). Additionally, the infiltration of groundwater through fault networks during the reactivation in the Late-Cretaceous

may have induced cementation of sediments and depressed the basin isotherms (Toupin et al., 1997), enhancing thermal conductivity of the sediments and thus inducing cooling by reducing thermal insulation (Takemura et al., 2017). Groundwater facilitated cooling may be especially relevant for the Eromanga Basin, as it hosts the regionally significant Great Artesian Basin within Jurassic–Cretaceous strata (Moya et al., 2015).

Thermal history models for the Dunoon 1 and Narcoonowie 1 wells to south of the Murteree Ridge suggest significantly different thermal histories compared to wells in the north. Southern wells preserve largely stable temperatures following deposition in the Winton Formation, notably appearing to have remained structurally buffered from middle Cretaceous hydrothermal circulation. Consequently, these wells do not display a rebound towards steady-state conditions once hydrothermal circulation ceased within the wider basin. The absence of Late-Cretaceous cooling south of the Murteree Ridge is further consistent with Eromanga Basin exhumation increasing from the southwest to the northeast (Mavromatidis & Hillis, 2005). Previous thermal history modelling of the Tinga Tingana 1 well in the southern Cooper Basin similarly indicates significantly lower magnitude of cooling during the Late-Cretaceous (Figure 7; Gravestock et al., 1998), as compared to wells further north. This is consistent with the compartmentalisation of troughs in the southern Cooper–Eromanga Basin which do not appear to have experienced as significant Cretaceous fault reactivation as observed to north of the Murteree Ridge, which has facilitated northward thickening of Eromanga Basin sediments (Kulikowski & Amrouch, 2018). The Pogona 1 well in the Wooloo Trough, to the north of the Murteree Ridge, similarly preserves no evidence for Late-Cretaceous cooling (Figure 7), suggesting this region also did not experience significant erosion following deposition of the Winton Formation.

## 5.2.3 | Cenozoic perturbation

Thermal history models for wells Pinna 1, Narcoonowie 1 and Moomba 1 and 72 provide evidence of an additional abrupt Cenozoic reheating event initiating sometime in the last ca. 30 Ma. While less clear from thermal history reconstruction, sample Po1-6 from the Pogona 1 well retains fossil tracks despite currently residing above the apatite partial annealing zone at a temperature of ca. 127°C (Ostler, 1990), which would imply this sample has only recently been brought to such temperatures. This secondary phase of late heating in the Eromanga Basin has also been observed in the Burley 2, Daralingie 1, Gidgelpa 1, Gidgelpa 5, Gidgelpa 7, Merrimelia 2, Merrimelia 4, Pando

1, Sturt 7 and Tinga Tingana 1 wells (Duddy et al., 2002; Duddy & Moore, 1999; McLaren & Dunlap, 2006), although the cause of reheating remains contentious. Thermal history models presented in this study are broadly consistent with previous AFT-based models proposed by Duddy et al. (2002), but show considerable variation in timing and rate of reheating. The models for the Pinna 1 and combined Moomba 1 and Moomba 72 wells (Figure 7) predict heating beginning in the last ca. 30 Ma, while abrupt heating at ca. 5–2 Ma in the Narcoonowie 1 well is more consistent with reheating described by Duddy et al. (2002).

While recent reheating signature has proved highly enigmatic, the presence of hot groundwater fluids within the Great Artesian Basin in excess of 120°C (e.g. Pirlo, 2004; Polak & Horsfall, 1979) invokes the possibility that the observed recent heating pulse is reflective of renewed hydrothermal activity, resulting in a change to the local geothermal regime. Hydrothermal activity in the basin may be attributed to reactivation of the Cooper Hot Spot in the Nappamerri Trough (Figure 7), which has commonly been associated with hydrothermal fluid circulation to the basin (Hardman et al., 2019; Röth & Littke, 2022). Notably, the westmost study wells (Dunoon 1 and Sturt 8) furthest from the Cooper Hot Spot do not exhibit recent reheating, suggesting hydrothermal cells may be confined close to this trough. Waters within the Great Artesian Basin have additionally recorded signatures of  $^3\text{He}$  proposed as magmatic mantle fluxes (e.g. Gallagher, 1988; Torgersen et al., 1992), which further suggest a history of mantle-related hydrothermal fluids which have contributed to elevated temperatures in the basin. Observed Neogene heating and potential relation to magmatic and hydrothermal does, however, still require further research to confidently resolve.

## 6 | CONCLUSIONS

This study provides the first combined AFT and apatite U–Pb thermochronology data from the Cooper–Eromanga Basin. Despite changes in the depositional environment, apatite provenance in the upper Eromanga Basin from ca. 150 to 90 Ma can be linked to syn-depositional volcanism on the east coast of Australia. The bulk of analysed apatites in the upper Eromanga Basin were likely sourced from the Whitsunday Igneous Association, with potential additional input from volcanogenic sediment recycled from the Gippsland, Otway and Bass Basins. An additional ca. 300–200 Ma apatite provenance was identified in the Winton, Mackunda and Cadnaowie Formations, likely sourced from the New England and/or Mossman Orogens. Post-depositional thermal histories appear strongly segregated between samples from north and south of the Murteree Ridge. Samples north of the

structure reflect significant heating at ca. 95–70 Ma following deposition of the Winton Formation, likely driven by hydrothermal activity and basal magmatic activity. Subsequent Late-Cretaceous cooling was likely driven by a combination of post-magmatic thermal subsidence, change in the hydrothermal regime, exhumation, and/or enhanced thermal conductivity by cementation. Wells south of the Murteree Ridge preserve much simpler thermal histories, and lack the Cretaceous hydrothermal circulation and associated heating pulse observed to the north. A recent Cenozoic reheating event within the last ca. 30 Ma is also widely preserved across the basin, which has been tentatively linked to renewed hydrothermal activity within the basin associated with reactivation of the Cooper Hot Spot.

## ACKNOWLEDGEMENTS

The authors acknowledge Sarah Gilbert for assistance with LA–ICP–MS data collection, and Barry Kohn and the University of Melbourne for providing access to a  $^{252}\text{Cf}$  irradiation source. Stijn Glorie is supported by an Australian Research Council Future Fellowship (FT210100906), Angus Nixon is supported by AuScope and the National Collaborative Research Infrastructure Strategy (NCRIS) as part of the AuScope Geochemistry Network. Open access publishing facilitated by The University of Adelaide, as part of the Wiley - The University of Adelaide agreement via the Council of Australian University Librarians.

## CONFLICT OF INTEREST STATEMENT

I declare there is no conflict of interest in the submission of this manuscript.

## PEER REVIEW

The peer review history for this article is available at <https://www.webofscience.com/api/gateway/wos/peer-review/10.1111/bre.12843>.

## DATA AVAILABILITY STATEMENT

The data that support the findings of this study are available through AusGeochem (<https://doi.org/10.58024/AGUADDD6D6B2>).

## ORCID

Angus L. Nixon  <https://orcid.org/0000-0003-3638-1864>  
Betina Bendell  <https://orcid.org/0000-0003-3372-3005>

## REFERENCES

- Alexander, E. M., & Hibburt, J. (1996). *The petroleum geology of South Australia: Volume 2—Eromanga Basin*. SA Department of Mines and Energy.
- Allen, C. M., Williams, I. S., Stephens, C. J., & Fielding, C. R. (1998). Granite genesis and basin formation in an extensional setting: The magmatic history of the Northernmost New England



- Orogen. *Australian Journal of Earth Sciences*, 45(6), 875–888. <https://doi.org/10.1080/08120099808728442>
- Apak, S. N., Stuart, W. J., Lemon, N. M., & Wood, G. (1997). Structural evolution of the Permian–Triassic Cooper Basin, Australia: Relation to hydrocarbon trap styles. *AAPG Bulletin*, 81(4), 533–555. <https://doi.org/10.1306/522b43c5-1727-11d7-8645000102c1865d>
- Armstrong, P. A. (2005). Thermochronometers in sedimentary basins. In P. W. Reiners & T. A. Ehlers (Eds.), *Low-temperature thermochronology: Techniques, interpretations, and applications* (pp. 499–525). Mineralogical Society of America.
- Barham, M., Kirkland, C. L., Reynolds, S., O'Leary, M. J., Evans, N. J., Allen, H., Haines, P. W., Hocking, R. M., McDonald, B. J., Belousova, E., & Goodall, J. (2016). The answers are blowin' in the wind: Ultra-distal ashfall zircons, indicators of Cretaceous super-eruptions in eastern Gondwana. *Geology*, 44(8), 643–646. <https://doi.org/10.1130/g38000.1>
- Beardsmore, G. (2004). The influence of basement on surface heat flow in the Cooper Basin. *Exploration Geophysics*, 35(4), 223–235. <https://doi.org/10.1071/EG04223>
- Beech, A. J. (1985). *Dunoon 1 well completion report*. Geological Survey of South Australia (WCR 06047) <https://sarigbasis.pir.sa.gov.au/WebtopEw/ws/samref/sarig1/image/DDD/DUNOO N001.zip>
- Black, L. P., McClenaghan, M. P., Korsch, R. J., Everard, J. L., & Foudoulis, C. (2005). Significance of Devonian–Carboniferous igneous activity in Tasmania as derived from U–Pb SHRIMP dating of zircon. *Australian Journal of Earth Sciences*, 52(6), 807–829. <https://doi.org/10.1080/08120090500304232>
- Boult, P. J., Theologou, P. M., & Foden, J. (1997). Capillary seals within the Eromanga Basin, Australia: Implications for exploration and production. *AAPG Memoir*, 67, 143–167.
- Bradshaw, B. E., Rollet, N., Iwanec, J., & Bernecker, T. (2022). A regional chronostratigraphic framework for play-based resource assessments in the Eromanga Basin. *The APPEA Journal*, 62, S392–S399. <https://doi.org/10.1071/AJ21097>
- Braz, C., Zahirovic, S., Salles, T., Flament, N., Harrington, L., & Müller, R. D. (2021). Modelling the role of dynamic topography and eustasy in the evolution of the Great Artesian Basin. *Basin Research*, 33(6), 3378–3405. <https://doi.org/10.1111/bre.12606>
- Bryan, S. E., Constantine, A. E., Stephens, C. J., Ewart, A., Schön, R. W., & Parianos, J. (1997). Early Cretaceous volcano-sedimentary successions along the eastern Australian continental margin: Implications for the break-up of eastern Gondwana. *Earth and Planetary Science Letters*, 153(1), 85–102. [https://doi.org/10.1016/S0012-821X\(97\)00124-6](https://doi.org/10.1016/S0012-821X(97)00124-6)
- Bryan, S. E., Cook, A. G., Allen, C. M., Siegel, C., Purdy, D. J., Greentree, J. S., & Uysal, I. T. (2012). Early-mid Cretaceous tectonic evolution of eastern Gondwana: From siliciclastic LIP magmatism to continental rapture. *Episodes*, 35(1), 142–152.
- Bryan, S. E., Ewart, A., Stephens, C. J., Parianos, J., & Downes, P. J. (2000). The Whitsunday Volcanic Province, Central Queensland, Australia: Lithological and stratigraphic investigations of a silicic-dominated large igneous province. *Journal of Volcanology and Geothermal Research*, 99(1), 55–78. [https://doi.org/10.1016/S0377-0273\(00\)00157-8](https://doi.org/10.1016/S0377-0273(00)00157-8)
- Cawood, P. A., Leitch, E. C., Merle, R. E., & Nemchin, A. A. (2011). Orogenesis without collision: Stabilizing the Terra Australis accretionary orogen, eastern Australia. *GSA Bulletin*, 123(11–12), 2240–2255. <https://doi.org/10.1130/b30415.1>
- Chaney, A. J., Cubitt, C. J., & Williams, B. P. J. (1997). Reservoir potential of glacio-fluvial sandstones: Merrimelia Formation, Cooper Basin, South Australia. *The APPEA Journal*, 37(1), 154–177. <https://doi.org/10.1071/AJ96009>
- Chew, D. M., O'Sullivan, G., Caracciolo, L., Mark, C., & Tyrrell, S. (2020). Sourcing the sand: Accessory mineral fertility, analytical and other biases in detrital U–Pb provenance analysis. *Earth-Science Reviews*, 202, 103093. <https://doi.org/10.1016/j.earscirev.2020.103093>
- Chew, D. M., Petrus, J. A., & Kamber, B. S. (2014). U–Pb LA-ICPMS dating using accessory mineral standards with variable common Pb. *Chemical Geology*, 363, 185–199. <https://doi.org/10.1016/j.chemgeo.2013.11.006>
- Chew, D. M., & Spikings, R. A. (2015). Geochronology and thermochronology using apatite: Time and temperature, lower crust to surface. *Elements*, 11(3), 189–194. <https://doi.org/10.2113/gselements.11.3.189>
- Cogné, N., Chew, D. M., Donelick, R. A., & Ansberque, C. (2020). LA-ICP-MS apatite fission track dating: A practical zeta-based approach. *Chemical Geology*, 531, 119302. <https://doi.org/10.1016/j.chemgeo.2019.119302>
- Collins, W. J. (1991). A reassessment of the 'Hunter-Bowen Orogeny': Tectonic implications for the southern New England fold belt. *Australian Journal of Earth Sciences*, 38(4), 409–423. <https://doi.org/10.1080/08120099108727981>
- Crook, K. A. W. (1980). Fore-arc evolution in the Tasman Geosyncline: The origin of the southeast Australian continental crust. *Journal of the Geological Society of Australia*, 27(1–2), 215–232. <https://doi.org/10.1080/00167618008729136>
- Deighton, I., & Hill, A. J. (1998). Thermal and burial history. In D. I. Gravestock, J. E. Hibbert, & J. F. Drexel (Eds.), *The petroleum geology of South Australia, volume 4* (pp. 143–153). SA Department of Mines and Energy.
- Donelick, R. A., & Miller, D. S. (1991). Enhanced TINT fission-track densities in low spontaneous track density apatites using <sup>252</sup>Cf-derived fission fragment tracks: A model and experimental observations. *Nuclear Tracks and Radiation Measurements*, 18(3), 301–307.
- Drexel, J. F., & Preiss, W. V. (1995). *The geology of South Australia, Volume 2*. Geological Survey of South Australia.
- Duddy, I. R., & Moore, M. E. (1999). *Thermal history reconstruction in Cooper-Eromanga Basin wells using apatite and zircon fission track analysis and vitrinite reflectance*. Geotrack International Report 668.
- Duddy, I. R., Moore, M. E., Marshallsea, S. J., & Green, P. F. (2002). *Provenance and thermal history studies in Cooper-Eromanga Basin wells*. Geotrack International.
- Ewart, A., Schon, R. W., & Chappell, B. W. (1992). The Cretaceous volcanic-plutonic province of the Central Queensland (Australia) coast—A rift related 'calc-alkaline' province. *Earth and Environmental Science Transactions of the Royal Society of Edinburgh*, 83(1–2), 327–345. <https://doi.org/10.1017/S0263593300008002>
- Fergusson, C. L., Fanning, C. M., Phillips, D., & Ackerman, B. R. (2005). Structure, detrital zircon U–Pb ages and <sup>40</sup>Ar/<sup>39</sup>Ar geochronology of the Early Palaeozoic Girilambone group, Central New South Wales: Subduction, contraction and extension associated with the Benambran orogeny. *Australian Journal of Earth Sciences*, 52(1), 137–159. <https://doi.org/10.1080/0812090500100044>



- Fergusson, C. L., & Henderson, R. A. (2015). Early Palaeozoic continental growth in the Tasmanides of Northeast Gondwana and its implications for Rodinia assembly and rifting. *Gondwana Research*, 28(3), 933–953. <https://doi.org/10.1016/j.gr.2015.04.001>
- Flowers, R. M., Farley, K. A., & Ketcham, R. A. (2015). A reporting protocol for thermochronologic modeling illustrated with data from the Grand Canyon. *Earth and Planetary Science Letters*, 432, 425–435. <https://doi.org/10.1016/j.epsl.2015.09.053>
- Foden, J., Elburg, M. A., Dougherty-Page, J., & Burt, A. (2006). The timing and duration of the Delamerian orogeny: Correlation with the Ross Orogen and implications for Gondwana assembly. *The Journal of Geology*, 114(2), 189–210. <https://doi.org/10.1086/499570>
- Frears, R. A. (1978). Narcoonowie 1 well completion report. Geological Survey of South Australia (WCR 03204) <https://sarigobasis.pir.sa.gov.au/WebtopEw/ws/samref/sarig1/image/DDD/NARCOONOWIE001.zip>
- Gallagher, K. (1988). *The subsidence history and thermal state of the Eromanga and Cooper basins*. PhD thesis, Australian National University, Canberra.
- Gallagher, K. (2012). Transdimensional inverse thermal history modeling for quantitative thermochronology. *Journal of Geophysical Research: Solid Earth*, 117, 1–16. <https://doi.org/10.1029/2011jb008825>
- Gatehouse, C. G., Fanning, C. M., & Flint, R. B. (1995). Geochronology of the Big Lake Suite, Warburton Basin, northeastern South Australia, Quarterly Geological Notes. *Geological Survey of South Australia*, 128, 8–16.
- Geological Survey of South Australia. (2022). SARIG. <https://map.sarig.sa.gov.au/>
- Gillespie, J., Glorie, S., Khudoley, A., & Collins, A. S. (2018). Detrital apatite U-Pb and trace element analysis as a provenance tool: Insights from the Yenisey ridge (Siberia). *Lithos*, 314–315, 140–155. <https://doi.org/10.1016/j.lithos.2018.05.026>
- Gleadow, A. J. W., Duddy, I. R., Green, P. F., & Lovering, J. F. (1986). Confined fission track lengths in apatite: A diagnostic tool for thermal history analysis. *Contributions to Mineralogy and Petrology*, 94(4), 405–415. <https://doi.org/10.1007/bf00376334>
- Gleadow, A. J. W., Gleadow, S. J., Belton, D. X., Kohn, B. P., Krochmal, M. S., & Brown, R. W. (2009). Coincidence mapping—A key strategy for the automatic counting of fission tracks in natural minerals. *Geological Society, London, Special Publications*, 324(1), 25–36. <https://doi.org/10.1144/sp324.2>
- Glorie, S., Alexandrov, I., Nixon, A., Jepson, G., Gillespie, J., & Jahn, B. M. (2017). Thermal and exhumation history of Sakhalin Island (Russia) constrained by apatite U-Pb and fission track thermochronology. *Journal of Asian Earth Sciences*, 143, 326–342. <https://doi.org/10.1016/j.jseas.2017.05.011>
- Glorie, S., March, S., Nixon, A., Meeuw, F., O'Sullivan, G. J., Chew, D. M., Kirkland, C. L., Konopelko, D., & De Grave, J. (2020). Apatite U–Pb dating and geochemistry of the Kyrgyz South Tian Shan (Central Asia): Establishing an apatite fingerprint for provenance studies. *Geoscience Frontiers*, 11(6), 2003–2015. <https://doi.org/10.1016/j.gsf.2020.06.003>
- Gravestock, D. I., Hibbert, J., & Drexel, J. F. (1998). *The petroleum geology of South Australia: Volume 4—Cooper Basin*. Geological Survey of South Australia.
- Gurnis, M., Müller, R. D., & Moresi, L. (1998). Cretaceous vertical motion of Australia and the Australian–Antarctic discordance. *Science*, 279(5356), 1499–1504. <https://doi.org/10.1126/science.279.5356.1499>
- Haines, P. W., Hand, M., & Sandiford, M. (2001). Palaeozoic synorogenic sedimentation in central and northern Australia: A review of distribution and timing with implications for the evolution of intracontinental orogens. *Australian Journal of Earth Sciences*, 48(6), 911–928. <https://doi.org/10.1046/j.1440-0952.2001.00909.x>
- Hall, L. S., Hill, A., Troup, A., Korsch, R., Radke, B., Nicoll, R. S., Palu, T., Wang, L., & Stacey, A. (2015). *Cooper Basin architecture and lithofacies: Regional hydrocarbon prospectivity of the Cooper Basin, part 1*. Geoscience Australia (Record 2015/31). <https://doi.org/10.11636/Record.2015.031>
- Hall, L. S., Palu, T. J., Murray, A. P., Boreham, C. J., Edwards, D. S., Hill, A. J., & Troup, A. (2019). Hydrocarbon prospectivity of the Cooper Basin, Australia. *AAPG Bulletin*, 103(1), 31–63. <https://doi.org/10.1306/05111817249>
- Hannaford, C., Young, M., Watts, C., Charles, A., Cooling, J., & Rollet, N. (2022). *Palynological data review of selected wells and new sampling results in the Great Artesian Basin*. Geoscience Australia (Record 2022/001). <https://doi.org/10.11636/Record.2022.001>
- Hardman, J. P. A., Holford, S. P., Schofield, N., Bunch, M., & Gibbins, D. (2019). The Warnie volcanic province: Jurassic intraplate volcanism in Central Australia. *Gondwana Research*, 76, 322–347. <https://doi.org/10.1016/j.gr.2019.06.012>
- Henderson, R. A., Innes, B. M., Fergusson, C. L., Crawford, A. J., & Withnall, I. W. (2011). Collisional accretion of a Late Ordovician oceanic island arc, northern Tasman orogenic zone, Australia. *Australian Journal of Earth Sciences*, 58(1), 1–19. <https://doi.org/10.1080/08120099.2010.535564>
- Idnurm, M., & Seno, B. R. (1978). Palaeomagnetic ages of late Cretaceous and tertiary weathered profiles in the Eromanga Basin, Queensland. *Palaeogeography, Palaeoclimatology, Palaeoecology*, 24(4), 263–277. [https://doi.org/10.1016/0031-0182\(78\)90010-X](https://doi.org/10.1016/0031-0182(78)90010-X)
- Jadoon, Q. K., Roberts, E. M., Henderson, B., Blenkinsop, T. G., Wüst, R. A. J., & Mtelela, C. (2017). Lithological and facies analysis of the Roseneath and Murteree shales, Cooper Basin, Australia. *Journal of Natural Gas Science and Engineering*, 37, 138–168. <https://doi.org/10.1016/j.jngse.2016.10.047>
- Kulikowski, D., & Amrouch, K. (2017). Combining geophysical data and calcite twin stress inversion to refine the tectonic history of subsurface and offshore provinces: A case study on the Cooper–Eromanga Basin, Australia. *Tectonics*, 36(3), 515–541. <https://doi.org/10.1002/2016TC004366>
- Kulikowski, D., & Amrouch, K. (2018). 3D seismic analysis investigating the relationship between stratigraphic architecture and structural activity in the intra-cratonic Cooper and Eromanga basins, Australia. *Marine and Petroleum Geology*, 91, 381–400. <https://doi.org/10.1016/j.marpetgeo.2018.01.019>
- Kulikowski, D., Amrouch, K., & Cooke, D. (2016). Geomechanical modelling of fault reactivation in the Cooper Basin, Australia. *Australian Journal of Earth Sciences*, 63(3), 295–314. <https://doi.org/10.1080/08120099.2016.1212925>
- Li, P. F., Rosenbaum, G., & Rubatto, D. (2012). Triassic asymmetric subduction rollback in the southern New England Orogen (eastern Australia): The end of the Hunter–Bowen orogeny.

- Australian Journal of Earth Sciences*, 59(6), 965–981. <https://doi.org/10.1080/08120099.2012.696556>
- Lloyd, J., Collins, A. S., Payne, J. L., Glorie, S., Holford, S. P., & Reid, A. J. (2016). Tracking the Cretaceous transcontinental Ceduna River through Australia: The hafnium isotope record of detrital zircons from offshore southern Australia. *Geoscience Frontiers*, 7(2), 237–244. <https://doi.org/10.1016/j.gsf.2015.06.001>
- MacDonald, J. D., Holford, S. P., Green, P. F., Duddy, I. R., King, R. C., & Backé, G. (2013). Detrital zircon data reveal the origin of Australia's largest delta system. *Journal of the Geological Society*, 170(1), 3–6. <https://doi.org/10.1144/jgs2012-093>
- Mavromatidis, A. (2006). Burial/exhumation histories for the Cooper–Eromanga Basins and implications for hydrocarbon exploration, Eastern Australia. *Basin Research*, 18(3), 351–373. <https://doi.org/10.1111/j.1365-2117.2006.00294.x>
- Mavromatidis, A. (2007). Exhumation study in the Cooper–Eromanga basins, Australia and the implications for hydrocarbon exploration. *Energy Sources, Part A: Recovery, Utilization, and Environmental Effects*, 29(7), 631–648. <https://doi.org/10.1080/009083190957775>
- Mavromatidis, A. (2008). Two layer model of lithospheric compression and uplift/exhumation in an intracratonic setting: An example from the Cooper–Eromanga basins, Australia. *International Journal of Earth Sciences*, 97(3), 623–634. <https://doi.org/10.1007/s00531-007-0260-5>
- Mavromatidis, A., & Hillis, R. (2005). Quantification of exhumation in the Eromanga Basin and its implications for hydrocarbon exploration. *Petroleum Geoscience*, 11(1), 79–92. <https://doi.org/10.1144/1354-079304-621>
- McDowell, F. W., McIntosh, W. C., & Farley, K. A. (2005). A precise Ar-40–Ar-39 reference age for the Durango apatite (U–Th)/He and fission-track dating standard. *Chemical Geology*, 214(3–4), 249–263. <https://doi.org/10.1016/j.chemgeo.2004.10.002>
- McLaren, S., & Dunlap, W. J. (2006). Use of  $^{40}\text{Ar}/^{39}\text{Ar}$  K-feldspar thermochronology in basin thermal history reconstruction: An example from the Big Lake Suite granites, Warburton Basin, South Australia. *Basin Research*, 18(2), 189–203. <https://doi.org/10.1111/j.1365-2117.2006.00288.x>
- McLaren, S., Sandiford, M., Powell, R., Neumann, N. L., & Woodhead, J. D. (2006). Palaeozoic intraplate crustal anatexis in the mount Painter Province, South Australia: Timing, thermal budgets and the role of crustal heat production. *Journal of Petrology*, 47, 2281–2302.
- Meixner, A. J., Kirkby, A. L., & Horspool, N. (2014). Using constrained gravity inversions to identify high-heat-producing granites beneath thick sedimentary cover in the Cooper Basin region of Central Australia. *Geothermics*, 51, 483–495. <https://doi.org/10.1016/j.geothermics.2013.10.010>
- Middleton, M. F. (1979). Heat flow in the Moomba, Big Lake and Toolachee gas fields of the Cooper Basin and implications for hydrocarbon maturation. *Exploration Geophysics*, 10(2), 149–155. <https://doi.org/10.1071/EG979149>
- Moore, P. S., & Elliott, P. (1980). *Pinna 1 well completion report*. Geological Survey of South Australia (WCR 03945). <https://sarigbasis.pir.sa.gov.au/WebtopEw/ws/samref/sarig1/image/DDD/PINNA001.zip>
- Moya, C. E., Raiber, M., Taulis, M., & Cox, M. E. (2015). Hydrochemical evolution and groundwater flow processes in the Galilee and Eromanga basins, Great Artesian Basin, Australia: A multivariate statistical approach. *Science of the Total Environment*, 508, 411–426. <https://doi.org/10.1016/j.scitotenv.2014.11.099>
- Munson, T. J. (2014). *Petroleum geology and potential of the on-shore Northern Territory, 2014* (pp. 1–242). Northern Territory Geological Survey (NTGS Report 22). <https://geoscience.nt.gov.au/gemis/ntgjsjpu/handle/1/81558>
- Norvick, M. S. (2005). *Plate tectonic reconstructions of Australia's southern margins*. Geoscience Australia (Record 2005/007). <https://pid.geoscience.gov.au/dataset/ga/61826>
- Ostler, S. (1990). *Pogona 1 well completion report*. Geological Survey of South Australia (WCR 07275/000) <https://sarigbasis.pir.sa.gov.au/WebtopEw/ws/samref/sarig1/image/DDD/POGON A001.zip>
- Ostler, S. (1993). *Moomba 72 well completion report*. Geological Survey of South Australia (WCR 07425/000) <https://mer-wcr.s3.amazonaws.com/2027707/MOOMBA072.zip>
- O'Sullivan, P. B., Kohn, B. P., Foster, D. A., & Gleadow, A. J. W. (1995). Fission track data from the Bathurst Batholith: Evidence for rapid mid-Cretaceous uplift and erosion within the eastern highlands of Australia. *Australian Journal of Earth Sciences*, 42(6), 597–607. <https://doi.org/10.1080/08120099508728228>
- O'Sullivan, P. B., & Parrish, R. R. (1995). The importance of apatite composition and single-grain ages when interpreting fission track data from plutonic rocks: A case study from the coast ranges, British Columbia. *Earth and Planetary Science Letters*, 132(1), 213–224. [https://doi.org/10.1016/0012-821X\(95\)00058-K](https://doi.org/10.1016/0012-821X(95)00058-K)
- Paton, C., Hellstrom, J., Paul, B., Woodhead, J., & Hergt, J. (2011). Iolite: Freeware for the visualisation and processing of mass spectrometric data. *Journal of Analytical Atomic Spectrometry*, 26(12), 2508–2518. <https://doi.org/10.1039/C1JA10172B>
- Pirlo, M. C. (2004). Hydrogeochemistry and geothermometry of thermal groundwaters from the Birdsville Track Ridge, Great Artesian Basin, South Australia. *Geothermics*, 33(6), 743–774. <https://doi.org/10.1016/j.geothermics.2004.07.001>
- Pochon, A., Poujol, M., Gloaguen, E., Branquet, Y., Cagnard, F., Gumiaux, C., & Gapais, D. (2016). U–Pb LA–ICP–MS dating of apatite in mafic rocks: Evidence for a major magmatic event at the Devonian–Carboniferous boundary in the Armorican Massif (France). *American Mineralogist*, 101(11), 2430–2442. <https://doi.org/10.2138/am-2016-5736>
- Polak, E. J., & Horsfall, C. L. (1979). Geothermal gradients in the Great Artesian Basin, Australia. *Exploration Geophysics*, 10(2), 144–148. <https://doi.org/10.1071/EG979144>
- Quentin de Gromard, R. (2013). The significance of E–W structural trends for the Alice Springs Orogeny in the Charters Towers Province, North Queensland. *Tectonophysics*, 587, 168–187. <https://doi.org/10.1016/j.tecto.2012.09.002>
- Reynolds, S. D., Mildren, S. D., Hillis, R. R., & Meyer, J. J. (2006). Constraining stress magnitudes using petroleum exploration data in the Cooper–Eromanga basins, Australia. *Tectonophysics*, 415(1), 123–140. <https://doi.org/10.1016/j.tecto.2005.12.005>
- Roberts, J., & Engel, B. A. (1987). Depositional and tectonic history of the southern New England Orogen. *Australian Journal of Earth Sciences*, 34(1), 1–20. <https://doi.org/10.1080/08120098708729391>
- Rosenbaum, G. (2018). The Tasmanides: Phanerozoic tectonic evolution of eastern Australia. *Annual Review of Earth and Planetary Sciences*, 46(1), 291–325. <https://doi.org/10.1146/annurev-earth-082517-010146>
- Rosenbaum, G., Li, P., & Rubatto, D. (2012). The contorted New England Orogen (eastern Australia): New evidence from U–Pb

- geochronology of early Permian granitoids. *Tectonics*, 31, TC1006. <https://doi.org/10.1029/2011tc002960>
- Röth, J. (2022). Thermo-tectonic evolution and source rock maturation in the Gippsland Basin (offshore Victoria) and in the central Eromanga Basin (Cooper region), Australia. PhD thesis, RWTH Aachen University <https://doi.org/10.18154/RWTH-2021-11953>
- Röth, J., & Littke, R. (2022). Down under and under cover - the tectonic and thermal history of the Cooper and Central Eromanga Basins (Central Eastern Australia). *Geosciences*, 12(3), 117. <https://doi.org/10.3390/geosciences12030117>
- Röth, J., Parent, A., Warren, C., Hall, L. S., Palmowski, D., Koronful, N., Husein, S. S., Sachse, V., & Littke, R. (2022). Lithospheric evolution, thermo-tectonic history and source-rock maturation in the Gippsland Basin, Victoria, southeastern Australia. *Australian Journal of Earth Sciences*, 69(1), 83–112. <https://doi.org/10.1080/08120099.2021.1938219>
- Schwebel, D. (1980). *Pelketa 1 well completion report*. Geological Survey of South Australia (WCR 03640). <https://sarigbasis.pir.sa.gov.au/WebtopEw/ws/samref/sarig1/image/DDD/PELKETA001.zip>
- Senior, B. R., Harrison, P. L., & Mond, A. (1978). *Geology of the Eromanga Basin* (Vol. 167). Bureau of Mineral Resources Geology and Geophysics, Bulletin.
- Siégel, C., Bryan, S., Purdy, D., Allen, C., Schrank, C., Uysal, T., Gust, D., & Beardsmore, G. (2012). Evaluating the role of deep granitic rocks in generating anomalous temperatures in south-West Queensland (pp. 95–102). Geological Survey of Queensland (Record 2012/14).
- Siégel, C., Bryan, S. E., Allen, C. M., Purdy, D. J., Cross, A. J., Uysal, I. T., & Gust, D. A. (2018). Crustal and thermal structure of the Thomson Orogen: Constraints from the geochemistry, zircon U–Pb age, and Hf and O isotopes of subsurface granitic rocks. *Australian Journal of Earth Sciences*, 65(7–8), 967–986. <https://doi.org/10.1080/08120099.2018.1447998>
- Siégel, C., Schrank, C. E., Bryan, S. E., Beardsmore, G. R., & Purdy, D. J. (2014). Heat-producing crust regulation of subsurface temperatures: A stochastic model re-evaluation of the geothermal potential in southwestern Queensland, Australia. *Geothermics*, 51, 182–200. <https://doi.org/10.1016/j.geothermics.2014.01.005>
- Sircombe, K. N. (1999). Tracing provenance through the isotope ages of littoral and sedimentary detrital zircon, eastern Australia. *Sedimentary Geology*, 124(1), 47–67. [https://doi.org/10.1016/S0037-0738\(98\)00120-1](https://doi.org/10.1016/S0037-0738(98)00120-1)
- Stephens, A., Reid, A., Hore, S., Gilmore, P., & Hill, S. (2017). Provenance of Mesozoic sediments in the southern Eromanga Basin, NSW: Implications for the source of placer gold of the Tibbooburra goldfields. *MESA Journal*, 84(3), 10–18.
- Takemura, T., Sato, M., Chiba, T., Uemura, K., Ito, Y., & Funabiki, A. (2017). Effect of sedimentary facies and geological properties on thermal conductivity of Pleistocene volcanic sediments in Tokyo, Central Japan. *Bulletin of Engineering Geology and the Environment*, 76(1), 191–203. <https://doi.org/10.1007/s10064-016-0856-8>
- Torgersen, T., Habermehl, M. A., & Clarke, W. B. (1992). Crustal helium fluxes and heat flow in the Great Artesian Basin, Australia. *Chemical Geology*, 102(1), 139–152. [https://doi.org/10.1016/0009-2541\(92\)90152-U](https://doi.org/10.1016/0009-2541(92)90152-U)
- Toupin, D., Eadington, P. J., Person, M., Morin, P., Wieck, J., & Warner, D. (1997). Petroleum hydrogeology of the Cooper and Eromanga basins, Australia: Some insights from mathematical modeling and fluid inclusion data. *AAPG Bulletin*, 81(4), 577–603. <https://doi.org/10.1306/522b43d9-1727-11d7-8645000102c1865d>
- Tucker, R. T., Roberts, E. M., Henderson, R. A., & Kemp, A. I. S. (2016). Large igneous province or long-lived magmatic arc along the eastern margin of Australia during the Cretaceous? Insights from the sedimentary record. *GSA Bulletin*, 128(9–10), 1461–1480. <https://doi.org/10.1130/b31337.1>
- Turner, M. (1991). *Sturt 8 well completion report*. Geological Survey of South Australia WCR 07312/000. <https://sarigbasis.pir.sa.gov.au/WebtopEw/ws/samref/sarig1/image/DDD/STURT008.zip>
- Veevers, J. J. (1984). Phanerozoic earth history of Australia. *Oxford Geological Science Series*, 2, 90–333.
- Veevers, J. J. (2000). Change of tectono-stratigraphic regime in the Australian plate during the 99 Ma (Mid-Cretaceous) and 43 Ma (Mid-Eocene) swerves of the Pacific. *Geology*, 28(1), 47–50. [https://doi.org/10.1130/0091-7613\(2000\)28<47:COTRIT>2.0.CO;2](https://doi.org/10.1130/0091-7613(2000)28<47:COTRIT>2.0.CO;2)
- Veevers, J. J., Powell, C. M., & Roots, S. R. (1991). Review of sea-floor spreading around Australia. 1. Synthesis of the patterns of spreading. *Australian Journal of Earth Sciences*, 38(4), 373–389. <https://doi.org/10.1080/08120099108727979>
- Vermeesch, P. (2017). Statistics for LA-ICP-MS based fission track dating. *Chemical Geology*, 456, 19–27. <https://doi.org/10.1016/j.chemgeo.2017.03.002>
- Vermeesch, P. (2018). IsoplotR: A free and open toolbox for geochronology. *Geoscience Frontiers*, 9(5), 1479–1493. <https://doi.org/10.1016/j.gsf.2018.04.001>
- Wagner, G. A., & Van den haute, P. (1992). *Fission-track dating*. Kluwer Academic Publishers.
- Watts, K. J. (1987). The Hutton Sandstone-Birkhead Formation transition, ATP 269P (1), Eromanga Basin. *The APPEA Journal*, 27(1), 215–229. <https://doi.org/10.1071/AJ86018>
- Whitford, D. J., Hamilton, P. J., & Scott, J. (1994). Sedimentary provenance studies in Australian basins using neodymium model ages. *The APPEA Journal*, 34(1), 320–329. <https://doi.org/10.1071/AJ93029>

## SUPPORTING INFORMATION

Additional supporting information can be found online in the Supporting Information section at the end of this article.

**How to cite this article:** Nixon, A. L., Fernie, N., Glorie, S., Hand, M., & Bendell, B. (2024). Thermal evolution and sediment provenance of the Cooper–Eromanga Basin: Insights from detrital apatite. *Basin Research*, 36, e12843. <https://doi.org/10.1111/bre.12843>